Euro. Jnl of Applied Mathematics (2009), *vol.* 20, *pp.* 187–214. © 2008 Cambridge University Press
doi:10.1017/S0956792508007766 Printed in the United Kingdom

Oscillatory instabilities and dynamics of multi-spike patterns for the one-dimensional Gray-Scott model

WAN CHEN and MICHAEL J. WARD

Department of Mathematics, University of British Columbia, Vancouver, Canada V6T 1Z2
email: ward@math.ubc.ca

(*Received 17 July 2007; revised 30 October 2008; first published online 4 December 2008*)

The dynamics and oscillatory instabilities of multi-spike solutions to the one-dimensional Gray-Scott reaction–diffusion system on a finite domain are studied in a particular parameter regime. In this parameter regime, a formal singular perturbation method is used to derive a novel ODE–PDE Stefan problem, which determines the dynamics of a collection of spikes for a multi-spike pattern. This Stefan problem has moving Dirac source terms concentrated at the spike locations. For a certain subrange of the parameters, this Stefan problem is quasi-steady and an explicit set of differential-algebraic equations characterizing the spike dynamics is derived. By analysing a nonlocal eigenvalue problem, it is found that this multi-spike quasi-equilibrium solution can undergo a Hopf bifurcation leading to oscillations in the spike amplitudes on an $O(1)$ time scale. In another subrange of the parameters, the spike motion is not quasi-steady and the full Stefan problem is solved numerically by using an appropriate discretization of the Dirac source terms. These numerical computations, together with a linearization of the Stefan problem, show that the spike layers can undergo a drift instability arising from a Hopf bifurcation. This instability leads to a time-dependent oscillatory behaviour in the spike locations.

1 Introduction

Localized spatio-temporal patterns consisting of spots have been observed in many physical and chemical experiments, including the ferrocyanide-iodate-sulphite reaction (cf. [25], the chloride-dioxide-malonic acid reaction (cf. [6]), and certain semi-conductor gas discharge systems (cf. [1, 2]). In these physical experiments, various dynamical behaviours and instabilities of spot patterns have been observed including breathing oscillations associated with either the spot amplitude or spot location, spot annihilation and spot self-replication. In order to theoretically determine the mechanisms underlying some of these instabilities, certain model reaction–diffusion systems with simple kinetics, such as the Gray-Scott model, have been proposed and shown numerically to qualitatively reproduce some of the intricate spot behaviour observed in physical experiments (cf. [5, 30, 37]). A survey of experimental and theoretical studies, through reaction–diffusion modeling, of localized patterns in various physical or chemical contexts is given in [42].

The Gray-Scott (GS) system models an irreversible reaction in a gel reactor where the reactor is maintained in contact with a reservoir of one of the two chemical species. In the

https://doi.org/10.1017/S0956792508007766 Published online by Cambridge University Press

one-dimensional domain $|x| < 1$, the dimensionless GS model in the singularly perturbed limit $\varepsilon > 0$ with $\varepsilon \to 0^+$ is (cf. [22] [29])

$$v_t = \epsilon^2 v_{xx} - v + \mathcal{A}uv^2, \qquad \tau u_t = Du_{xx} + (1-u) - \epsilon^{-1}uv^2, \qquad u_x = v_x = 0, \quad x = \pm 1. \tag{1.1}$$

Here $\mathcal{A} > 0$ is the feed-rate parameter, $\tau > 0$ is the reaction-time parameter, and $D > 0$ with $D = O(1)$.

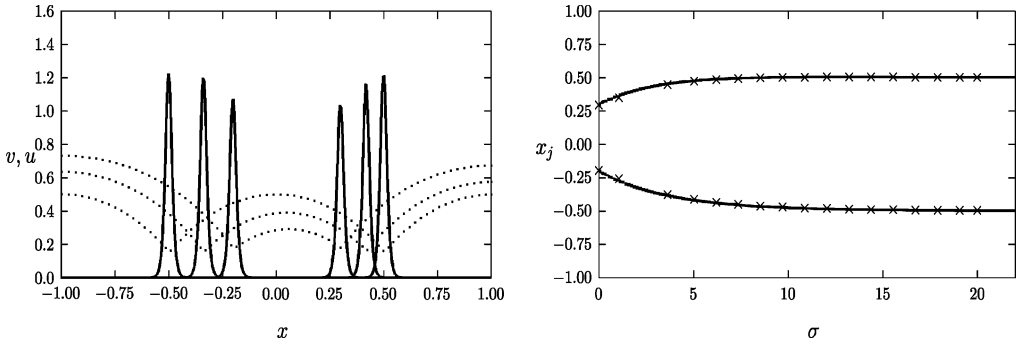
The pioneering numerical study of [37] for the GS model in a two-dimensional spatial domain, which showed a diverse range of dynamical behaviours of spot patterns, has stimulated much theoretical work to analyse and classify the full range of dynamical behaviour and instabilities of spike solutions for the more tractable one-dimensional GS model (1.1) in the limit $\varepsilon \to 0$. These studies include self-replication behaviour in the regime $D = O(\varepsilon^2)$ (cf. [33, 41]) and in the regime $D = O(1)$ (cf. [9, 23, 29, 38]), spatial temporal chaos for $D = O(\varepsilon^2)$ (cf. [34]), the existence and stability of equilibrium spike patterns for $D = O(1)$ (cf. [9, 10, 22, 24, 27, 28]), and the slow dynamics of spike patterns (cf. [7, 8, 39]).

More generally, there have been several formal asymptotic studies of spike motion for two-component singularly perturbed reaction–diffusion systems in the limit of small diffusivity of only one of the two species. These include, two-spike dynamics for the GS model on the infinite domain (cf. [7, 8]), k-spike dynamics with $k \geqslant 1$ for an elliptic-parabolic limit of the Gierer-Meinhardt (GM) model (cf. [17]), two-spike dynamics for a class of problems including a regularized GM model on the infinite line (cf. [11]), and two-spike dynamics for the GM model and for the GS model in the low feed-rate regime $\mathcal{A} = O(1)$ on a finite domain (cf. [39]). Recently, in [12] a renormalization method was used to rigorously analyse two-spike dynamics for a regularized GM model on the infinite line.

The goal of this paper is to analyse the dynamics and oscillatory instabilities of multi-spike solutions to the GS model (1.1) in the intermediate regime $O(1) \ll \mathcal{A} \ll O(\varepsilon^{-1/2})$ of the feed-rate parameter $\mathcal{A}$. The novelty and significance of this intermediate parameter regime is that, in terms of the reaction-time parameter τ, there are two distinct sub-regimes in $\mathcal{A}$ where qualitatively different types of spike dynamics and instabilities occur. These instabilities represent either a breathing instability in the spot amplitude, or a breathing instability in the spot location. In addition, in the intermediate parameter regime a formal singular perturbation analysis, as summarized in Principal Result 2.1, reveals that an ODE–PDE coupled Stefan-type problem with moving Dirac source terms determines the time-dependent locations of the spike trajectories. The derivation and study of this Stefan problem is a new result for spike dynamics in the GS model. Finally, in contrast to previous studies, our study is not limited to the special case of two-spike dynamics. In our analysis, we can readily treat an arbitrary number of spikes for (1.1) in the regime $O(1) \ll \mathcal{A} \ll O(\varepsilon^{-1/2})$.

In the subregime $O(1) \ll \mathcal{A} \ll O(\epsilon^{-1/3})$ with $\tau \ll O(\varepsilon^{-2}\mathcal{A}^{-2})$, the Stefan problem is quasi-steady and we derive an explicit differential-algebraic (DAE) system for the spike trajectories. The result is given in Principal Result 2.2. For the case of a two-spike evolution, in Figure 1 we illustrate our result by plotting the quasi-equilibrium solution for u and v together with the spike trajectories for a particular set of the parameter values. In this figure, the asymptotic DAE system results for the spike trajectories are

https://doi.org/10.1017/S0956792508007766 Published online by Cambridge University Press



(a) v and u vs. x (b) x_j vs. σ

FIGURE 1. Slow dynamics, for $\varepsilon = 0.01$, $\mathcal{A} = 8$, and $D = 0.2$, of a two-spike quasi-equilibrium solution with $x_1(0) = -0.2$ and $x_2(0) = 0.3$. Left figure: plot of v (solid curves) and u (dotted curves) versus x at $\sigma = 0$, $\sigma = 2.5$, and $\sigma = 30$. Right figure: plot of x_j versus $\sigma = \varepsilon^2\mathcal{A}^2 t$. As σ increases, the spikes drift to their steady state limits at $x = \pm 1/2$. The solid curves are the asymptotic results and the crosses indicate full numerical results computed from (1.1) using the software of [4].

shown to compare very favourably with full numerical results computed from (1.1) using the method of [4]. In this sub-regime, where the speed of the spikes is $O(\varepsilon^2\mathcal{A}^2) \ll 1$, we show from the analysis of a non-local eigenvalue problem (NLEP) that the instantaneous quasi-equilibrium spike solution first loses its stability to a Hopf bifurcation in the spike amplitudes when $\tau = \tau_H = O(\mathcal{A}^4)$. This bifurcation leads to oscillations on an $O(1)$ time scale in the amplitudes of the spikes. Our stability results are given in Principal Results 3.1 and 3.2. These NLEP stability results are the first such results for multi-spike quasi-equilibrium patterns for the GS model on a finite domain with an arbitrary number of spikes. An important remark is that our NLEP stability analysis in the intermediate regime for a multi-spike pattern with $O(1)$ inter-spike distances can be reduced to the study of a *single* NLEP. This feature, which greatly simplifies the stability analysis, is in distinct contrast to the stability analysis of [39] and [22] for the GS model in the low feed-rate regime $\mathcal{A} = O(1)$, and for the corresponding Gierer-Meinhardt model (see [12, 17, 43]), where k -distinct NLEP's govern the stability of k-spike patterns.

Next, we study spike dynamics in the sub-regime $O(\epsilon^{-1/3}) \ll \mathcal{A} \ll O(\epsilon^{-1/2})$ with $\tau = \tau_0\varepsilon^{-2}\mathcal{A}^{-2}$, for some $O(1)$ bifurcation parameter τ_0. In this regime, the time-dependent spike locations are determined from the full numerical solution of a Stefan-type problem with moving Dirac source terms concentrated at the unknown spike locations. Similar moving boundary problems arise in the study of the immersed boundary method (see [3, 40]). The numerical method that we use for our Stefan problem relies on the approach of [40] involving a high-order spatial discretization of singular Dirac source terms. Such high-spatial accuracy is needed in our problem in order to accurately calculate the average flux for u at each source point, which determines the speed of each spike. An explicit time integration scheme is then used to advance the spike trajectories each time step. With this numerical approach we compute large-scale time-dependent oscillatory motion in the spike locations when the reaction-time parameter τ_0 exceeds some critical bifurcation value. Although the overall scheme has a high spatial order of accuracy, the explicit

https://doi.org/10.1017/S0956792508007766 Published online by Cambridge University Press

time integration step renders our numerical scheme not particularly suitable for studying large-scale drift instabilities over very long time intervals.

By linearizing the Stefan problem around an equilibrium spike solution, we analytically calculate a critical value of τ_0 at which the equilibrium solution becomes unstable to small-scale oscillations in the equilibrium spike location. This bifurcation value of τ_0, given in Proposition 4.1 below, sets the threshold value for an oscillatory drift instability. The result for τ_0, based on a linearization of the Stefan problem, agrees with the result derived in [24] using the singular limit eigenvalue problem (SLEP) method of [31].

The SLEP method has been extensively used to study similar oscillatory drift instabilities that lead to the destabilization of equilibrium transition layer solutions for FitzHugh–Nagumo type systems (cf. [16, 32]). With this method, Hopf bifurcation values for the onset of the instability can be calculated and the dominant translation instability, either zigzag or breather, can be identified (cf. [32]). For spatially extended systems on the infinite line, it is then often possible to perform a centre manifold reduction, valid near the Hopf bifurcation point, to develop a weakly nonlinear normal form theory for large-scale oscillatory drift instabilities (see [13, 14] and the references therein). In contrast to this normal form theory, we emphasize that our Stefan problem with moving sources provides a description of large-scale oscillatory drift instabilities for values of τ_0 not necessarily close to the Hopf bifurcation point.

Similar Stefan problems with moving Dirac source terms have appeared in a few other contexts. In particular, such a problem determines a flame-front interface in the thin reaction zone limit of a certain PDE model of solid fuel combustion on the infinite line (cf. [36]). By using the heat kernel, this Stefan problem was reformulated in [36] into a nonlinear integrodifferential equation for the moving flame-front interface. By solving this integrodifferential equation numerically, a periodic doubling cascade and highly irregular relaxation oscillations of the flame-front interface were computed in [36]. For a related Stefan problem arising from solid combustion theory, a three-term Galerkin-type truncation was used in [15] to qualitatively approximate the Stefan problem by a more tractable finite dimensional dynamical system, which can then be readily analysed. Finally, we remark that in [19] a time-dependent moving source with prescribed speed was shown to prevent blowup behaviour for a certain class of nonlinear heat equation.

An outline of this paper is as follows. In Section 2 we derive the Stefan problem governing spike dynamics in the intermediate regime $O(1) \ll \mathcal{A} \ll O(\varepsilon^{-1/2})$. In Section 2.1 we analyse the quasi-steady limit of this problem. In Section 3 we analyse the stability of the quasi-equilibrium spike patterns of Section 2.1 in the sub-regime $O(1) \ll \mathcal{A} \ll O(\varepsilon^{-1/3})$. In Section 4 we compute numerical solutions to the Stefan problem showing large-scale oscillatory drift instabilities in the subregime $O(\varepsilon^{-1/3}) \ll \mathcal{A} \ll O(\varepsilon^{-1/2})$. In addition, a critical value of τ_0 for the onset of this instability is determined analytically. Concluding remarks are made in Section 5.

2 The dynamics of k-spike quasi-equilibria: A Stefan problem

In this section, we first derive the ODE–PDE Stefan problem that determines the time-dependent trajectories of the spike locations for (1.1) in the intermediate regime $O(1) \ll \mathcal{A} \ll O(\varepsilon^{-1/2})$.

https://doi.org/10.1017/S0956792508007766 Published online by Cambridge University Press

To do so we first motivate the scalings of u, v and the slow time that are needed for describing spike dynamics when $O(1) \ll \mathcal{A} \ll O(\varepsilon^{-1/2})$. In the inner region, we introduce a scaling such that $\mathcal{A}uv = O(1)$, with $v = O(\mathcal{A})$ as suggested by the equilibrium theory of section 4 of [22]. We also introduce the slow time $\sigma = \sigma_0 t$, with $\sigma_0 \ll 1$. With $v = \mathcal{A}v_j$, $u = u_j/\mathcal{A}^2$, and $y = \varepsilon^{-1}[x - x_j(\sigma)]$, where $\sigma = \sigma_0 t$, (1.1) becomes

$$-\varepsilon^{-1}\sigma_0 \frac{\mathrm{d}x_j}{\mathrm{d}\sigma} v_j' = v_j'' - v_j + u_j v_j^2, \quad -\frac{\sigma_0 \tau}{\mathcal{A}^2}\left(\frac{\mathrm{d}x_j}{\mathrm{d}\sigma}\right) u_j' = \frac{D}{\varepsilon \mathcal{A}^2} u_j'' + \varepsilon\left(1 - \frac{u_j}{\mathcal{A}^2}\right) - u_j v_j^2, \quad (2.1)$$

where the primes on u_j and v_j indicate derivatives in y. The equation for u_j suggests that $u_j = u_{j0} + O(\varepsilon \mathcal{A}^2)$, where u_{j0} is a constant. This enforces from the v_j equation that $v_j = v_{j0} + O(\varepsilon \mathcal{A}^2)$, and $\sigma_0 = \varepsilon^2 \mathcal{A}^2$. Since u_j is independent of y to leading order, the left-hand side of the u_j equation can be neglected only when $\sigma_0 \tau \varepsilon \mathcal{A}^2/\mathcal{A}^2 \ll 1$. With $\sigma_0 = \varepsilon^2 \mathcal{A}^2$, this condition is satisfied only when $\tau \varepsilon^3 \mathcal{A}^2 \ll 1$.

This simple scaling argument suggests that we expand the solution in the jth inner region as

$$u = \frac{1}{\mathcal{A}^2}[u_{0j} + \varepsilon \mathcal{A}^2 u_{1j} + \cdots], \qquad v = \mathcal{A}[v_{0j} + \varepsilon \mathcal{A}^2 v_{1j} + \cdots], \quad (2.2a)$$

where $u_{mj} = u_{mj}(y, \sigma)$ and $v_{mj}(y, \sigma)$ depend on the inner variable y and the slow time σ defined by

$$y \equiv \varepsilon^{-1}[x - x_j(\sigma)], \qquad \sigma \equiv \varepsilon^2 \mathcal{A}^2 t. \quad (2.2b)$$

Upon substituting (2.2) into (1.1), and assuming that $\tau \varepsilon^3 \mathcal{A}^2 \ll 1$, we obtain the leading-order problem

$$v_{0j}'' - v_{0j} + u_{0j} v_{0j}^2 = 0, \qquad u_{0j}'' = 0, \qquad -\infty < y < \infty. \quad (2.3)$$

At next order, we obtain

$$v_{1j}'' - v_{1j} + 2u_{0j} v_{0j} v_{1j} = -u_{1j} v_{0j}^2 - x_j' v_{0j}', \qquad D u_{1j}'' = u_{0j} v_{0j}^2, \qquad -\infty < y < \infty. \quad (2.4)$$

From (2.3) we take u_{0j} to be independent of y. The leading-order solution is then written as

$$u_{0j} = \frac{1}{\gamma_j}, \qquad v_{0j} = \gamma_j w, \quad (2.5)$$

where $\gamma_j = \gamma_j(\sigma)$, referred to as the amplitude of the jth spike, is to be found. Here $w(y)$ satisfies

$$w'' - w + w^2 = 0, \quad -\infty < y < \infty; \qquad w(\pm\infty) = 0, \quad w(0) > 0, \quad w'(0) = 0. \quad (2.6)$$

The unique homoclinic of (2.6) is $w = \frac{3}{2}\mathrm{sech}^2(y/2)$. Therefore, from (2.4), we get on $-\infty < y < \infty$ that

$$\mathcal{L} v_{1j} \equiv v_{1j}'' - v_{1j} + 2w v_{1j} = -\gamma_j^2 w^2 u_{1j} - x_j' \gamma_j w', \qquad D u_{1j}'' = \gamma_j w^2. \quad (2.7)$$

https://doi.org/10.1017/S0956792508007766 Published online by Cambridge University Press

Since $\mathcal{L}w' = 0$, the solvability condition for v_{ij} in (2.7) yields that

$$x_j' \int_{-\infty}^{\infty} (w')^2 \, \mathrm{d}y = -\frac{\gamma_j}{3} \int_{-\infty}^{\infty} u_{1j} \frac{\mathrm{d}}{\mathrm{d}y}(w^3) \, \mathrm{d}y. \tag{2.8}$$

Upon integrating (2.8) by parts twice, and noting that w and u_{1j}'' are even functions of y, we obtain

$$x_j' \int_{-\infty}^{\infty} (w')^2 \, \mathrm{d}y = \frac{\gamma_j}{6} [u_{1j}'(+\infty) + u_{1j}'(-\infty)] \int_{-\infty}^{\infty} w^3 \, \mathrm{d}y. \tag{2.9}$$

The explicit form of w is then used to evaluate the integrals in (2.9) to get

$$x_j' = \gamma_j [u_{1j}'(+\infty) + u_{1j}'(-\infty)], \qquad j = 1, \ldots, k. \tag{2.10}$$

Now consider the outer region defined where $|x - x_j| = O(1)$ for $j = 1, \ldots, k$. Since the term $\varepsilon^{-1} u v^2$ in (1.1) is localized near each $x = x_j$, its effect on the outer solution for u can be calculated in the sense of distributions. From (2.2a), and $\int_{-\infty}^{\infty} w^2 \, \mathrm{d}y = 6$, we obtain that $\epsilon^{-1} u v^2 \to \sum_{j=1}^{k} \gamma_j (\int_{-\infty}^{\infty} w^2 \, \mathrm{d}y) \delta(x - x_j) = \sum_{j=1}^{k} 6\gamma_j \delta(x - x_j)$. This leads to the outer problem for $u(x, \sigma)$ given by

$$\tau \varepsilon^2 \mathcal{A}^2 u_\sigma = D u_{xx} + (1 - u) - \sum_{j=1}^{k} 6\gamma_j \, \delta(x - x_j), \qquad |x| \leqslant 1,$$

with $u_x = 0$ at $x = \pm 1$. The matching condition between the inner and outer solutions for u yields

$$u(x_j(\sigma), \sigma) = \frac{1}{\gamma_j \mathcal{A}^2} \ll 1, \qquad u_x(x_j^{\pm}(\sigma), \sigma) = u_{1j}'(\pm\infty). \tag{2.11}$$

We summarize our asymptotic construction as follows:

Principal Result 2.1 *Assume that $\tau \varepsilon^3 \mathcal{A}^2 \ll 1$. Then, in the intermediate regime $O(1) \ll \mathcal{A} \ll O(\varepsilon^{-1/2})$, the GS model (1.1) can be reduced to the coupled ODE–PDE Stefan problem*

$$\tau \varepsilon^2 \mathcal{A}^2 u_\sigma = D u_{xx} + (1 - u) - \sum_{j=1}^{k} 6\gamma_j \, \delta(x - x_j), \qquad |x| \leqslant 1, \tag{2.12a}$$

$$\frac{\mathrm{d}x_j}{\mathrm{d}\sigma} = \gamma_j [u_x(x_j^+, \sigma) + u_x(x_j^-, \sigma)], \qquad j = 1, \ldots, k, \tag{2.12b}$$

$$u(x_j(\sigma), \sigma) = \frac{1}{\gamma_j \mathcal{A}^2}, \qquad j = 1, \ldots, k, \tag{2.12c}$$

with $u_x(\pm 1, \sigma) = 0$. Here $\sigma = \varepsilon^2 \mathcal{A}^2 t$ is the slow time scale, and $x_j(\sigma)$ is the centre of the jth spike.

We observe that (2.12a) is a heat equation with singular Dirac source terms, and that (2.12b) become explicit ODE's only when we can determine $u_x(x_j^{\pm}, \sigma)$ analytically. Finally, the constraints in (2.12c) implicitly determine the spike amplitudes $\gamma_j(\sigma)$, for $j = 1, \ldots, k$. As a remark, the interface motion in (2.12b) resulting from the average of the flux of u_x across the interface differs from that of the classic Stefan moving boundary problem (cf. [35]) from mathematical theories of phase change that involve the difference in the flux of u_x across the interface.

https://doi.org/10.1017/S0956792508007766 Published online by Cambridge University Press

2.1 Multi-spike quasi-equilibria: The quasi-steady limit $\tau\varepsilon^2\mathcal{A}^2 \ll 1$

We suppose that $\tau \ll \varepsilon^{-2}\mathcal{A}^{-2}$ so that u in (2.12a) is quasi-steady. With this assumption, we readily calculate from (2.12a), together with $u_x = 0$ at $x = \pm 1$, that

$$u = \begin{cases} 1 - g_1 \dfrac{\cosh(\theta(x+1))}{\cosh(\theta(x_1+1))}, & -1 \leqslant x < x_1 \\ 1 - g_j \dfrac{\sinh(\theta(x_{j+1}-x))}{\sinh(\theta(x_{j+1}-x_j))} - g_{j+1}\dfrac{\sinh(\theta(x-x_j))}{\sinh(\theta(x_{j+1}-x_j))}, & x_j \leqslant x \leqslant x_{j+1}, \quad j=1,\ldots,k-1, \\ 1 - g_k \dfrac{\cosh(\theta(1-x))}{\cosh(\theta(1-x_k))}, & x_k < x \leqslant 1\,. \end{cases} \tag{2.13}$$

Here $\theta \equiv D^{-1/2}$ and $u = 1 - g_j$ at $x = x_j$. From this solution we calculate u_x as $x \to x_j^{\pm}$, and we impose the required jump conditions $[Du_x]_j = 6\gamma_j$ for $j = 1,\ldots,k$ as seen from (2.12a). Here $[\zeta]_j \equiv \zeta(x_j^+) - \zeta(x_j^-)$. This leads to the matrix problem

$$\mathcal{B}\mathbf{g} = \frac{6}{\sqrt{D}}\Gamma\,\mathbf{e}, \tag{2.14}$$

where the matrices $\mathcal{B}$ and Γ and the vectors $\mathbf{g}$ and $\mathbf{e}$ are defined by

$$\mathcal{B} \equiv \begin{pmatrix} c_1 & d_1 & 0 & \cdots & 0 \\ d_1 & c_2 & d_2 & \cdots & 0 \\ \vdots & \ddots & \ddots & \ddots & \vdots \\ 0 & \cdots & d_{k-2} & c_{k-1} & d_{k-1} \\ 0 & \cdots & 0 & d_{k-1} & c_k \end{pmatrix}, \quad \Gamma \equiv \begin{pmatrix} \gamma_1 & \cdots & 0 \\ \vdots & \ddots & \vdots \\ 0 & \cdots & \gamma_k \end{pmatrix},$$
$$\mathbf{g} \equiv \begin{pmatrix} g_1 \\ \vdots \\ g_k \end{pmatrix}, \quad \mathbf{e} \equiv \begin{pmatrix} 1 \\ \vdots \\ 1 \end{pmatrix}. \tag{2.15}$$

The matrix entries of $\mathcal{B}$ are given explicitly by

$$\begin{gathered} c_1 = \coth(\theta(x_2-x_1)) + \tanh(\theta(1+x_1)), \qquad c_k = \coth(\theta(x_k - x_{k-1})) + \tanh(\theta(1-x_k)), \\ c_j = \coth(\theta(x_{j+1}-x_j)) + \coth(\theta(x_j - x_{j-1})), \quad \text{for } j = 2,\ldots,k-1, \\ d_j = -\operatorname{csch}(\theta(x_{j+1}-x_j)), \qquad \text{for } j = 1,\ldots,k-1. \end{gathered} \tag{2.16}$$

Next, we write the constraint (2.12c) in matrix form and combine it with (2.14) to get

$$\mathbf{g} = \mathbf{e} - \frac{1}{\mathcal{A}^2}\Gamma^{-1}\mathbf{e}\,. \qquad \gamma = \frac{\sqrt{D}}{6}\left(\mathcal{B}\mathbf{e} - \frac{1}{\mathcal{A}^2}\mathcal{B}\Gamma^{-1}\mathbf{e}\right), \tag{2.17}$$

where $\gamma \equiv (\gamma_1,\ldots,\gamma_k)^t$. Since Γ^{-1} depends on γ, (2.17) is a nonlinear algebraic system for the spike amplitudes γ_j for $j = 1,\ldots,k$. For $\mathcal{A} \gg 1$, (2.17) reduces asymptotically to the two-term result

$$\gamma = \frac{\sqrt{D}}{6}\mathcal{B}\left(I - \frac{6}{\mathcal{A}^2\sqrt{D}}\Gamma_0^{-1}\right)\mathbf{e} + O(\mathcal{A}^{-4}), \tag{2.18}$$

https://doi.org/10.1017/S0956792508007766 Published online by Cambridge University Press

where I is the identity matrix. Here Γ_0^{-1} is the inverse of the diagonal matrix Γ_0 defined by

$$\Gamma_0 \equiv \begin{pmatrix} (\mathcal{B}\mathbf{e})_1 & \cdots & 0 \\ \vdots & \ddots & \vdots \\ 0 & \cdots & (\mathcal{B}\mathbf{e})_k \end{pmatrix}, \tag{2.19}$$

where $(\mathcal{B}\mathbf{e})_j$ denotes the jth component of the vector $\mathcal{B}\mathbf{e}$. Upon using the identity $\coth\mu - \operatorname{csch}\mu = \tanh(\mu/2)$, we can write (2.18) component-wise as

$$\gamma_j = \frac{\sqrt{D}}{6}(\mathcal{B}\mathbf{e})_j\left(1 - \frac{6}{\mathcal{A}^2\sqrt{D}}r_j\right) + O(\mathcal{A}^{-4}), \qquad r_j \equiv \frac{\left(\mathcal{B}\Gamma_0^{-1}\mathbf{e}\right)_j}{(\mathcal{B}\mathbf{e})_j}, \tag{2.20a}$$

where

$$(\mathcal{B}\mathbf{e}) = \begin{pmatrix} \tanh\left(\frac{\theta}{2}(x_2 - x_1)\right) + \tanh\left(\theta(1 + x_1)\right) \\ \vdots \\ \tanh\left(\frac{\theta}{2}(x_j - x_{j-1})\right) + \tanh\left(\frac{\theta}{2}(x_{j+1} - x_j)\right) \\ \vdots \\ \tanh\left(\frac{\theta}{2}(x_k - x_{k-1})\right) + \tanh\left(\theta(1 - x_k)\right) \end{pmatrix}. \tag{2.20b}$$

With this approximation, and since $\Gamma^{-1} \sim \frac{6}{\sqrt{D}}\Gamma_0^{-1}$ for $\mathcal{A} \gg 1$, (2.17) for $\mathbf{g}$ reduces asymptotically to

$$\mathbf{g} = \mathbf{e} - \frac{6}{\mathcal{A}^2\sqrt{D}}\,\Gamma_0^{-1}\mathbf{e} + O(\mathcal{A}^{-4}). \tag{2.21}$$

This asymptotically determines the unknown constants g_j for $j = 1, \ldots, k$ in (2.13) with an error $O(\mathcal{A}^{-4})$.

Next, we derive an explicit form for the ODE's in (2.12b). By calculating $u_x(x_j^{\pm})$ from (2.13), we readily derive that $\mathbf{x}' = (x_1', \ldots, x_k')^t$ satisfies

$$\mathbf{x}' = -\frac{1}{\sqrt{D}}\Gamma\,\mathcal{Q}\,\mathbf{g}, \tag{2.22}$$

where $\mathcal{Q}$ is the tridiagonal matrix defined by

$$\mathcal{Q} \equiv \begin{pmatrix} e_1 & f_1 & 0 & \cdots & 0 \\ -f_1 & e_2 & f_2 & \cdots & 0 \\ \vdots & \ddots & \ddots & \ddots & \vdots \\ 0 & \cdots & -f_{k-2} & e_{k-1} & f_{k-1} \\ 0 & \cdots & 0 & -f_{k-1} & e_k \end{pmatrix}, \tag{2.23a}$$

with matrix entries

$$\begin{aligned} e_1 &= -\coth(\theta(x_2 - x_1)) + \tanh(\theta(1 + x_1)), \quad e_k = \coth(\theta(x_k - x_{k-1})) - \tanh(\theta(1 - x_k)), \\ e_j &= -\coth(\theta(x_{j+1} - x_j)) + \coth(\theta(x_j - x_{j-1})), \quad \text{for } j = 2, \ldots, k-1, \\ f_j &= \operatorname{csch}(\theta(x_{j+1} - x_j)), \qquad \text{for } j = 1, \ldots, k-1. \end{aligned} \tag{2.23b}$$

https://doi.org/10.1017/S0956792508007766 Published online by Cambridge University Press

Finally, by combining (2.22) and (2.17), we obtain the following asymptotic result for the dynamics of k-spike quasi-equilibria:

Principal Result 2.2 *Assume that* $\tau\varepsilon^2\mathcal{A}^2 \ll 1$ *and* $O(1) \ll \mathcal{A} \ll O(\varepsilon^{-1/2})$. *Then, the quasi-equilibrium solution to (1.1) for* $v(x,\sigma)$ *is*

$$v(x,\sigma) \sim \mathcal{A}\sum_{j=1}^{k} \gamma_j w[\varepsilon^{-1}(x - x_j(\sigma))], \tag{2.24}$$

where $w(y) = 3/2sech^2\left(y/2\right)$. *The corresponding outer approximation for* u *is given in (2.13) where the coefficients* g_j *in (2.13) for* $j = 1,\ldots,k$ *are given asymptotically in (2.21). For* $\mathcal{A} \gg 1$, *the spike amplitudes* $\gamma_j(\sigma)$ *are given asymptotically in terms of the instantaneous spike locations* x_j *by (2.20a). Finally, the vector of spike locations satisfy the ODE system*

$$\frac{\mathrm{d}\mathbf{x}}{\mathrm{d}\sigma} \sim -\frac{1}{\sqrt{D}}\Gamma\,\mathcal{Q}\left(I - \frac{6}{\mathcal{A}^2\sqrt{D}}\Gamma_0^{-1}\right)\mathbf{e}, \tag{2.25}$$

with $\sigma = \varepsilon^2\mathcal{A}^2 t$. *Here* Γ_0 *is defined in (2.19) and* Γ *is defined in (2.15).*

The equilibrium positions of the spikes satisfy $\Gamma\ \mathcal{Q}\mathbf{g} = 0$. In equilibrium, γ_j is a constant independent of j, and hence $\mathbf{g} = c\mathbf{e}$ where c is some constant. Consequently, the equilibrium spike locations satisfy $\mathcal{Q}\mathbf{e} = \mathbf{0}$. By using (2.23), this leads to $x_j = -1 + (2j-1)/k$ for $j = 1,\ldots,k$.

The leading-order approximation for the ODE's in (2.25) is obtained by using $\Gamma \sim \frac{\sqrt{D}}{6}\Gamma_0 + O(\mathcal{A}^{-2})$, and $\mathbf{g} \sim \mathbf{e} + O(\mathcal{A}^{-2})$. With this approximation, which neglects the $O(\mathcal{A}^2)$ terms, (2.25) reduces to

$$\begin{aligned}
x_1' &\sim -\frac{1}{6}\left(\tanh^2\left[\theta(1+x_1)\right] - \tanh^2\left[\frac{\theta}{2}(x_2 - x_1)\right]\right),\\
x_j' &\sim -\frac{1}{6}\left(\tanh^2\left[\frac{\theta}{2}(x_j - x_{j-1})\right] - \tanh^2\left[\frac{\theta}{2}(x_{j+1} - x_j)\right]\right), \qquad j = 1,\ldots,k-1,\\
x_k' &\sim -\frac{1}{6}\left(\tanh^2\left[\frac{\theta}{2}(x_k - x_{k-1})\right] - \tanh^2\left[\theta(1-x_k)\right]\right).
\end{aligned} \tag{2.26}$$

3 Oscillatory profile instabilities of k-spike quasi-equilibria

We now analyse the stability of the k-spike quasi-equilibrium solution of Section 2.1 to instabilities occurring on a fast $O(1)$ time scale. Since the spike locations drift slowly with speed $O(\varepsilon^2\mathcal{A}^2)$ (cf. (2.25)), in our stability analysis we make the asymptotic approximation that the spikes are at some fixed locations $x_1,\ldots,x_k$. This asymptotic separation of time scales with 'frozen' spike locations allows for the derivation of an NLEP governing fast instabilities.

Let u_e and v_e be the quasi-equilibrium solution constructed in Section 2.1. We substitute $u(x,t) = u_e + e^{\lambda t}\eta(x)$ and $v(x,t) = v_e + e^{\lambda t}\phi(x)$ into (1.1), and then linearize to obtain

$$\epsilon^2\phi_{xx} - \phi + 2\mathcal{A}u_e v_e\phi + \mathcal{A}v_e^2\eta = \lambda\phi, \qquad |x| \leqslant 1\,; \qquad \phi_x(\pm 1) = 0, \tag{3.1a}$$

$$D\eta_{xx} - (1+\tau\lambda)\,\eta - \varepsilon^{-1}v_e^2\eta = 2\varepsilon^{-1}u_e v_e\phi, \qquad |x| \leqslant 1\,; \qquad \eta_x(\pm 1) = 0. \tag{3.1b}$$

https://doi.org/10.1017/S0956792508007766 Published online by Cambridge University Press

We then look for a localized eigenfunction for ϕ in the form

$$\phi(x) = \sum_{j=1}^{k} \phi_j[\varepsilon^{-1}(x - x_j)], \tag{3.2}$$

with $\phi_j \to 0$ as $|y| \to \infty$. Since $v_e \sim \mathcal{A}\gamma_j w$ and $u_e \sim 1/(\gamma_j \mathcal{A}^2)$ near $x = x_j$, we obtain from (3.1a) that $\phi_j(y)$ satisfies

$$\phi_j'' - \phi_j + 2w\phi_j + \mathcal{A}^3\gamma_j^2 w^2 \eta(x_j) = \lambda\phi_j, \qquad -\infty < y < \infty. \tag{3.3}$$

Next, we consider (3.1b). Since ϕ_j is localized near each spike, the spatially inhomogeneous coefficients in (3.1b) can be approximated by Dirac masses. In this way, and by using $v_e \sim \mathcal{A}\gamma_j w$, $u_e \sim 1/(\gamma_j\mathcal{A}^2)$, and $\int_{-\infty}^{\infty} w^2\,\mathrm{d}y = 6$, we obtain for x near x_j that $2\varepsilon^{-1}u_e v_e \phi \sim 2/\mathcal{A}(\int_{-\infty}^{\infty} w\phi_j\,\mathrm{d}y)\delta(x - x_j)$ and $\varepsilon^{-1}v_e^2 \sim 6\mathcal{A}^2\gamma_j^2\delta(x - x_j)$. Therefore, the outer problem for η in (3.1b) becomes

$$D\eta_{xx} - \left[1 + \tau\lambda + 6\mathcal{A}^2 \sum_{j=1}^{k} \gamma_j^2\,\delta(x - x_j)\right]\eta = \sum_{j=1}^{k} \frac{2}{\mathcal{A}} \left(\int_{-\infty}^{+\infty} w\phi_j\,\mathrm{d}y\right)\delta(x - x_j), \tag{3.4}$$

with $\eta_x = 0$ at $x = \pm 1$. Defining $[\xi]_j$ by $[\xi]_j \equiv \xi(x_{j+}) - \xi(x_{j-})$, we obtain the equivalent problem

$$D\eta_{xx} - (1 + \tau\lambda)\eta = 0, \quad |x| \leqslant 1\,; \qquad \eta_x(\pm 1) = 0, \tag{3.5a}$$

$$[\eta]_j = 0, \quad [D\eta_x]_j = -6\omega_j + 6\mathcal{A}^2\gamma_j^2\eta(x_j), \quad j = 1, \ldots, k\,; \qquad \omega_j \equiv -\frac{2}{\mathcal{A}}\left(\frac{\int_{-\infty}^{\infty} w\phi_j\,\mathrm{d}y}{\int_{-\infty}^{\infty} w^2\,\mathrm{d}y}\right). \tag{3.5b}$$

Next, we calculate $\eta_j \equiv \eta(x_j)$ from (3.5), which is needed in (3.3). To do so, we solve (3.5a) on each sub-interval and then use the jump conditions in (3.5b). This leads to the matrix problem

$$\mathcal{E}_\lambda \boldsymbol{\eta} = \frac{6}{[D(1 + \tau\lambda)]^{1/2}}\boldsymbol{\omega}, \tag{3.6}$$

where the vectors $\boldsymbol{\omega}$ and $\boldsymbol{\eta}$ are defined by $\boldsymbol{\omega}^t = (\omega_1, \ldots, \omega_k)$ and $\boldsymbol{\eta}^t = (\eta_1, \ldots, \eta_k)$, and where t denotes transpose. The matrix $\mathcal{E}_\lambda$ in (3.6) is defined in terms of a tridiagonal matrix $\mathcal{B}_\lambda$ by

$$\mathcal{E}_\lambda \equiv \mathcal{B}_\lambda + \frac{6\mathcal{A}^2}{\sqrt{D(1 + \tau\lambda)}}\,I^2, \qquad \mathcal{B}_\lambda \equiv \begin{pmatrix} c_{1,\lambda} & d_{1,\lambda} & 0 & \cdots & 0 \\ d_{1,\lambda} & \ddots & \ddots & \ddots & \vdots \\ 0 & \ddots & \ddots & \ddots & 0 \\ \vdots & \ddots & \ddots & \ddots & d_{k-1,\lambda} \\ 0 & \cdots & 0 & d_{k-1,\lambda} & c_{k,\lambda} \end{pmatrix}. \tag{3.7}$$

https://doi.org/10.1017/S0956792508007766 Published online by Cambridge University Press

Here Γ is the diagonal matrix of spike amplitudes defined in (2.15). The matrix entries of $\mathcal{B}_\lambda$ are

$$c_{1,\lambda} = \coth(\theta_\lambda(x_2 - x_1)) + \tanh(\theta_\lambda(1 + x_1)), \quad c_{k,\lambda} = \coth(\theta_\lambda(x_k - x_{k-1}) + \tanh(\theta_\lambda(1 - x_k)),$$
$$c_{j,\lambda} = \coth(\theta_\lambda(x_{j+1} - x_j)) + \coth(\theta_\lambda(x_j - x_{j-1})), \quad j = 2,\ldots,k-1, \tag{3.8}$$
$$d_{j,\lambda} = -\operatorname{csch}(\theta_\lambda(x_{j+1} - x_j)), \quad j = 1,\ldots,k-1\,.$$

In (3.8), θ_λ is the principal branch of the square root for $\theta_\lambda \equiv \theta_0\sqrt{1+\tau\lambda}$, with $\theta_0 \equiv D^{-1/2}$. Notice that when $\lambda = 0$, $\mathcal{B}_\lambda = \mathcal{B}$, where $\mathcal{B}$ was defined in (2.15).

Next, we invert (3.6) to obtain

$$\boldsymbol{\eta} = \frac{1}{[D(1+\tau\lambda)]^{1/2}}\mathcal{E}_\lambda^{-1}\boldsymbol{\omega} = -\frac{12}{\mathcal{A}\sqrt{D(1+\tau\lambda)}}\left(\frac{\int_{-\infty}^{\infty} w\,(\mathcal{E}_\lambda^{-1}\boldsymbol{\phi})\,\mathrm{d}y}{\int_{-\infty}^{\infty} w^2\,\mathrm{d}y}\right), \tag{3.9}$$

where $\boldsymbol{\phi}^t = (\phi_1,\ldots,\phi_k)$. Substituting (3.9) into (3.3), we obtain the following NLEP in terms of a new matrix $\mathcal{C}_\lambda$:

$$\boldsymbol{\phi}'' - \boldsymbol{\phi} + 2w\boldsymbol{\phi} - w^2\left(\frac{\int_{-\infty}^{\infty} w\,(\mathcal{C}_\lambda\boldsymbol{\phi})\,\mathrm{d}y}{\int_{-\infty}^{\infty} w^2\,\mathrm{d}y}\right) = \lambda\boldsymbol{\phi}\,; \qquad \mathcal{C}_\lambda \equiv \frac{12\mathcal{A}^2}{\sqrt{D(1+\tau\lambda)}}\Gamma^2\mathcal{E}_\lambda^{-1}. \tag{3.10}$$

Since Γ is a positive definite diagonal matrix and $\mathcal{E}_\lambda$ is symmetric, we can decompose $\mathcal{C}_\lambda$ as

$$\mathcal{C}_\lambda = \mathcal{S}\mathcal{X}\mathcal{S}^{-1}, \tag{3.11}$$

where $\mathcal{X}$ is the diagonal matrix of eigenvalues χ_j of $\mathcal{C}_\lambda$ and $\mathcal{S}$ is the matrix of its eigenvectors $\boldsymbol{s}_j$. We then set $\boldsymbol{\psi} = \mathcal{S}^{-1}\boldsymbol{\phi}$ to diagonalize (3.10), and we rewrite $\mathcal{C}_\lambda$ in terms of $\mathcal{B}_\lambda$ by using (3.7). This leads to the following stability criterion for $O(1)$ time-scale instabilities:

Principal Result 3.1 *The k-spike quasi-equilibrium solution of § 2.1 with fixed spike locations is stable on a fast $O(1)$ time scale if the following k NLEP's on $-\infty < y < \infty$, given by*

$$\psi'' - \psi + 2w\psi - \chi_j(\tau\lambda)w^2\left(\frac{\int_{-\infty}^{\infty} w\psi\,\mathrm{d}y}{\int_{-\infty}^{\infty} w^2\,\mathrm{d}y}\right) = \lambda\psi\,; \qquad \psi \to 0 \quad \text{as} \quad |y| \to \infty, \tag{3.12}$$

only have eigenvalues with $\mathrm{Re}(\lambda) < 0$. Here $\chi_j(\tau\lambda)$ for $j = 1,\ldots,k$ are the eigenvalues of the matrix C_λ defined by

$$\mathcal{C}_\lambda = 2\left[I + \frac{\sqrt{D(1+\tau\lambda)}}{6\mathcal{A}^2}\mathcal{B}_\lambda\Gamma^{-2}\right]^{-1}. \tag{3.13}$$

We now analyse (3.12). Let $\tau = O(1)$ and assume that the inter-spike distances $d_j = x_{j+1} - x_j$ for $j = 0,\ldots,k$ are $O(1)$. Here, for $j = 0$ and $j = k$ we define $d_0 = x_1 + 1$ and $d_k = 1 - x_k$, respectively. Then, for $\mathcal{A} \gg 1$, (3.13) yields $C_\lambda \sim 2I$ so that $\chi_j \sim 2$ for $j = 1,\ldots,k$. Since χ_j is a constant with $\chi_j > 1$ in this limit, the result of Theorem 1.4 of [44] proves that $\mathrm{Re}(\lambda) < 0$. This guarantees stability for $\mathcal{A} \gg 1$ when $\tau = O(1)$ and $d_j = x_{j+1} - x_j = O(1)$.

https://doi.org/10.1017/S0956792508007766 Published online by Cambridge University Press

Next, we consider the limit $\mathcal{A} \gg 1$, $\tau = O(1)$, but we will allow for the inter-spike distances $d_j = x_{j+1} - x_j$ to be small but with $d_j \gg O(\varepsilon)$. Recall that the analysis of Section 2 and Section 3 leading to Principal Result 3.1 required that $d_j \gg O(\varepsilon)$. We will show that for the scaling regime $d_j = O(\mathcal{A}^{-2/3}) \gg O(\varepsilon)$ of closely spaced spikes, and with $O(1) \ll \mathcal{A} \ll O(\varepsilon^{-1/2})$, the NLEP (3.12) can have an unstable eigenvalue for any $\tau > 0$. For simplicity, we will only consider a closely spaced equilibrium configuration with $d_j = L \ll 1$ for $j = 1, \ldots, k-1$, and $d_0 = d_k = L/2$. In this limit it is readily shown from (3.8) that

$$\mathcal{B}_\lambda \sim \frac{1}{\theta_\lambda L}\mathcal{B}_0, \qquad \mathcal{B}_0 \equiv \begin{pmatrix} 1 & -1 & 0 & \cdots & 0 \\ -1 & 2 & -1 & \cdots & 0 \\ \vdots & \ddots & \ddots & \ddots & \vdots \\ 0 & \cdots & -1 & 2 & -1 \\ 0 & \cdots & 0 & -1 & 1 \end{pmatrix}. \tag{3.14}$$

Moreover, for $\mathcal{A} \gg 1$ and with spikes of a uniform spacing $L \ll 1$, we obtain from (2.20) that the spikes have a common amplitude given by

$$\gamma_j \sim \frac{\sqrt{D}}{6}(\mathcal{B}e)_j = \frac{\sqrt{D}}{3}\tanh\left(\frac{\theta_0 L}{2}\right) \sim \frac{L}{6}. \tag{3.15}$$

Substituting (3.14) and (3.15) into (3.13), we obtain that the eigenvalues χ_j of C_λ are given by

$$\chi_j \sim 2\left[1 + \frac{\sqrt{D(1+\tau\lambda)}}{6\mathcal{A}^2}\left(\frac{36}{L^2}\right)\left(\frac{r_j}{\theta_\lambda L}\right)\right]^{-1} = 2\left[1 + \frac{6Dr_j}{\mathcal{A}^2 L^3}\right]^{-1}, \tag{3.16}$$

where r_j for $j = 1, \ldots, k$ are the eigenvalues of the matrix $\mathcal{B}_0$ defined in (3.14). Appendix E of [18] and Theorem 1.4 of [44] prove that when χ_j is constant, then $\mathrm{Re}(\lambda) > 0$ if and only if $\chi_j < 1$ for $j = 1, \ldots, k$.

The stability threshold is determined by $\chi_m \equiv \min_{j=1,\ldots,k}(\chi_j) = 1$, which depends on the largest eigenvalue $r_m \equiv \max_{j=1,\ldots,k}(r_j)$ of $\mathcal{B}_0$. By calculating r_m and setting $\chi_m = 1$, we obtain that the k-spike equilibrium solution is unstable for any $\tau > 0$ on the regime $O(1) \ll \mathcal{A} \ll O(\varepsilon^{-1/2})$ when $L < L_*$, where

$$L_* \equiv \left(\frac{6Dr_m}{\mathcal{A}^2}\right)^{1/3}, \qquad r_m \equiv 2[1 + \cos(\pi/k)]. \tag{3.17}$$

The result (3.17) shows that competition instabilities in the intermediate regime $O(1) \ll \mathcal{A} \ll O(\varepsilon^{-1/2})$ can only occur if the spikes are sufficiently close with inter-spike separation $O(\mathcal{A}^{-2/3})$. If we did set $\mathcal{A} = O(1)$ in (3.17), then $L_* = O(1)$ is consistent with the scalings in [22] and [39] for competition instabilities of equilibrium and quasi-equilibrium spike patterns in the low feed-rate regime $\mathcal{A} = O(1)$.

Next, we obtain our main instability result that oscillatory instabilities of k-spike quasi-equilibria can occur when $\tau = O(\mathcal{A}^4) \gg 1$ and with $O(1)$ inter-spike separation distances. From the choice of the principal value of the square root, we obtain that $\mathrm{Re}(\theta_\lambda) = \theta_0 \mathrm{Re}(\sqrt{1+\tau\lambda}) \to +\infty$ on $|\arg(\lambda)| < \pi$ as $\tau \to \infty$. Therefore, for $\tau \gg 1$, and for $x_{j+1} - x_j = O(1)$, we calculate from the matrix entries of $\mathcal{B}_\lambda$ in (3.8) that $\mathcal{B}_\lambda \to 2I$ in

https://doi.org/10.1017/S0956792508007766 Published online by Cambridge University Press

$|\arg(\lambda)| < \pi$. Therefore, with $\tau = \tilde{\tau}\mathcal{A}^4$, where $\tilde{\tau} = O(1)$, we get from (3.13) that C_λ and its eigenvalues χ_j are given asymptotically by

$$\mathcal{C}_\lambda \sim 2\left[I + \frac{\sqrt{D\tilde{\tau}\lambda}}{3}\Gamma^{-2}\right]^{-1}; \qquad \chi_j \sim 2\left[1 + \frac{\sqrt{D\tilde{\tau}\lambda}}{3}\gamma_j^{-2}\right]^{-1} \quad \text{for} \quad j = 1,\ldots,k. \tag{3.18}$$

This limiting expression for χ_j suggests that we define τ_H by $\tilde{\tau} = 9D^{-1}\gamma_j^4\tau_H$, so that $\mathcal{C} \sim 2[1 + \sqrt{\tau_H\lambda}]^{-1}I$. Therefore, in the scaling regime $\tau = O(\mathcal{A}^4)$, the stability of k-spike quasi-equilibria is determined by the NLEP (3.12) with the single multiplier

$$\chi_\infty = \frac{2}{1 + \sqrt{\tau_H\lambda}}, \qquad \text{when} \quad \tau = \frac{9\mathcal{A}^4\tau_H\gamma_j^4}{D} \gg 1. \tag{3.19}$$

This limiting NLEP was derived for equilibrium spike solutions in [9, 10, 22, 28] in the intermediate regime. From the rigorous analysis of [10] and [22], this NLEP has a Hopf bifurcation at some $\tau_H = \tau_{H0}$. From numerical computations, $\tau_{H0} \approx 1.748$, and $\mathrm{Re}(\lambda) < 0$ only when $\tau_H < \tau_{H0}$ (cf. [9, 22]). Although, this limiting NLEP has a continuous spectrum on the non-negative real axis $\mathrm{Re}(\lambda) \leqslant 0$, there are no edge bifurcations arising from the end-point $\lambda = 0$ (cf. [10, 22]).

The scaling law for τ in (3.19) shows that there are k distinct values of τ where complex conjugate eigenvalues appear on the imaginary axis. The minimum of these values determines the instability threshold for τ. Finally, by using (2.20) to calculate the spike amplitudes asymptotically for $\mathcal{A} \gg 1$, we obtain the following main instability result:

Principal Result 3.2 *Let $\tau = O(\mathcal{A}^4)$ with $x_{j+1} - x_j = O(1)$ and $O(1) \ll \mathcal{A} \ll O(\varepsilon^{-1/2})$. Then, the frozen k-spike quasi-equilibrium solution of Section 2.1 develops an oscillatory instability due to a Hopf bifurcation when τ increases past τ_h, where*

$$\tau_h = \min_{j=1,\ldots,k}(\tau_{hj}), \qquad \tau_{hj} \sim \frac{D\mathcal{A}^4}{144}\tau_{H0}\,(\mathcal{B}\mathbf{e})_j^4\left(1 - \frac{6}{\mathcal{A}^2\sqrt{D}}r_j\right)^4, \qquad j = 1,\ldots,k\,. \tag{3.20}$$

Here $\tau_{H0} \approx 1.748$, while $(\mathcal{B}\mathbf{e})_j$ and r_j are defined in terms of the spike locations by (2.20).

For an equilibrium k-spike pattern where $x_j = -1 + (2j-1)/k$ for $j = 1,\ldots,k$, we calculate from (2.20b) that $(\mathcal{B}\mathbf{e})_j = 2\tanh(\theta_0/k)$ and $r_j = [2\tanh(\theta_0/k)]^{-1}$ for $j = 1,\ldots,k$. This leads to the following equilibrium stability threshold, which agrees asymptotically with that given in Proposition 4.3 of [22].:

$$\tau_h \sim \frac{D\mathcal{A}^4}{9}\tau_{H0}\tanh^4\left(\frac{\theta_0}{k}\right)\left(1 - \frac{3}{\mathcal{A}^2\sqrt{D}\tanh\left(\theta_0/k\right)}\right)^4, \tag{3.21}$$

An important remark concerns the range of validity of Principal Result 3.2 with respect to τ. The derivation of (3.20) assumed that $\tau\varepsilon^2\mathcal{A}^2 \ll 1$, while the scaling law for instabilities predicts that $\tau = O(\mathcal{A}^4)$. Thus, (3.20) only holds in the sub-regime $O(1) \ll \mathcal{A} \ll O(\varepsilon^{-1/3})$ of the intermediate regime.

https://doi.org/10.1017/S0956792508007766 Published online by Cambridge University Press

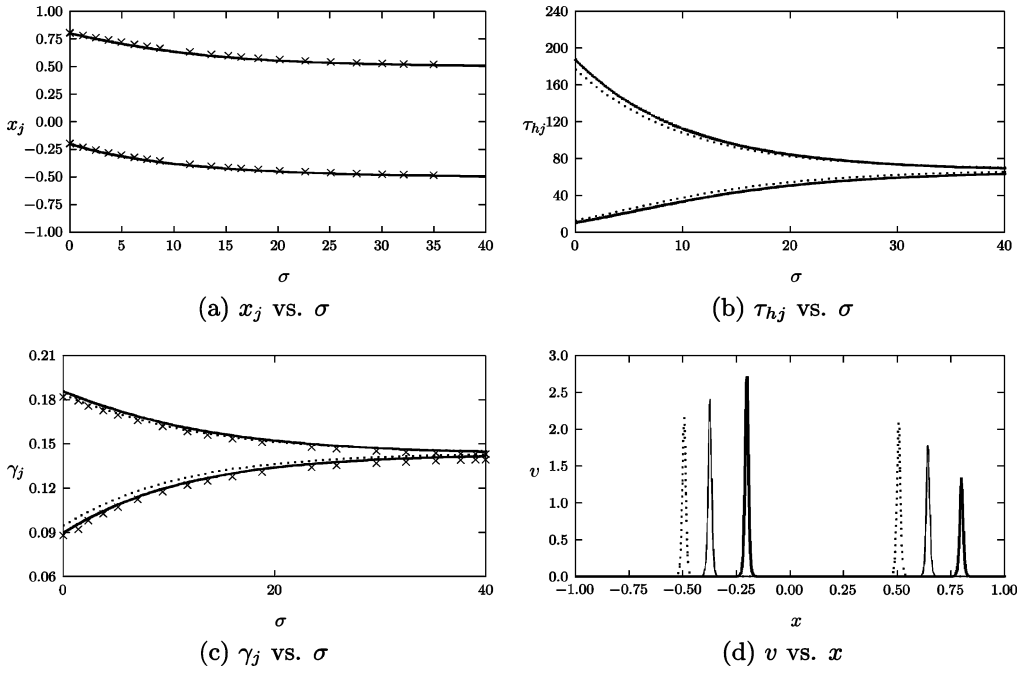


FIGURE 2. *Experiment 3.1:* Slow evolution of a two-spike quasi-equilibrium solution for $\varepsilon = 0.005$, $\mathcal{A} = 10$ and $D = 1.0$, with $x_1(0) = -0.2$ and $x_2(0) = 0.8$. Top Left: x_j versus σ. Top Right: τ_{hj} versus σ. Bottom Left: γ_j versus σ. Bottom Right: v versus x at $\sigma = 0$ (heavy solid curve), $\sigma = 10$ (solid curve) and $\sigma = 50$ (dotted curve). Except for the plot of v versus x, the solid curves correspond to computing the spike amplitudes from (2.17), while the dotted curves correspond to the two-term approximation (2.18). The crosses in the plots of x_j and γ_j versus σ are the full numerical results computed from (1.1).

3.1 Numerical experiments of quasi-equilibrium spike layer motion

We now give two examples illustrating our results of Sections 2 and 3 for slow spike dynamics.

Experiment 3.1: A two-spike evolution

Consider a two-spike evolution with parameter values $D = 1.0$, $\mathcal{A} = 10.0$, $\tau = 5.0$, and $\varepsilon = 0.005$. The initial spike locations are $x_1(0) = -0.20$ and $x_2(0) = 0.80$. In Figure 2(a) we plot the spike layer trajectories versus the slow time σ, computed numerically from (2.25), which shows the gradual approach to the equilibrium values at $x_1 = -1/2$ and $x_2 = 1/2$. In Figure 2(c) we plot the spike amplitudes versus σ. A plot of the quasi-equilibrium solution at several instants in time is shown in Figure 2(d). In Figure 2(b) we plot the two Hopf bifurcation values τ_{hj}, for $j = 1, 2$, versus σ calculated from (3.20). In these figures, the solid curves were obtained when computing for the spike amplitudes from the nonlinear algebraic system (2.17), while the dotted curves correspond to using the two-term approximation (2.18). For the spike trajectories shown in Figure 2(a) these two curves are indistinguishable. In the plots of the spike locations and spike amplitudes in

https://doi.org/10.1017/S0956792508007766 Published online by Cambridge University Press

Figure 2(a) and Figure 2(c), the marked points are the full numerical results computed from (1.1) using the adaptive-grid software of [4]. From these figures we observe that the asymptotic and full numerical results agree very closely. An important observation from Figure 2(b) is that the stability threshold $\tau_h(\sigma)$, defined by $\tau_h(\sigma) \equiv \min_{j=1,2}[\tau_{hj}(\sigma)]$, is an increasing function of σ with $\tau_h(0) \approx 12.5$ and $\tau_h(\infty) \approx 67.7$. This monotone behaviour of $\tau_h(\sigma)$, together with the initial value $\tau_h(0) > \tau = 5.0$, implies that there is no dynamic triggering of an oscillatory instability in the spike amplitudes before the equilibrium two-spike pattern is reached.

More generally, we have been unable to prove analytically from the DAE system (2.25) and (2.18) that the stability threshold $\tau_h(\sigma) \equiv \min_{j=1,\ldots,k}(\tau_{hj}(\sigma))$ of (3.20) must always be an increasing function of σ. However, we have performed many numerical experiments to examine this condition, and in each case we have found numerically that $\tau_h(\sigma)$ is a monotonically increasing function of σ. This leads to the conjecture that there are no dynamically triggered oscillatory instabilities of multi-spike quasi-equilibria in the intermediate regime $O(1) \ll \mathcal{A} \ll O(\varepsilon^{-1/2})$. In other words, $\tau < \tau_h(0)$ is a sufficient condition for stability of the quasi-equilibrium multi-spike pattern for all $\sigma > 0$. In contrast, for the simple case of symmetric two-spike quasi-equilibria in the low feed-rate regime $\mathcal{A} = O(1)$, dynamically triggered instabilities due to either Hopf bifurcations or from the creation of a real positive eigenvalue were established analytically in [39].

Experiment 3.2: A three-spike evolution

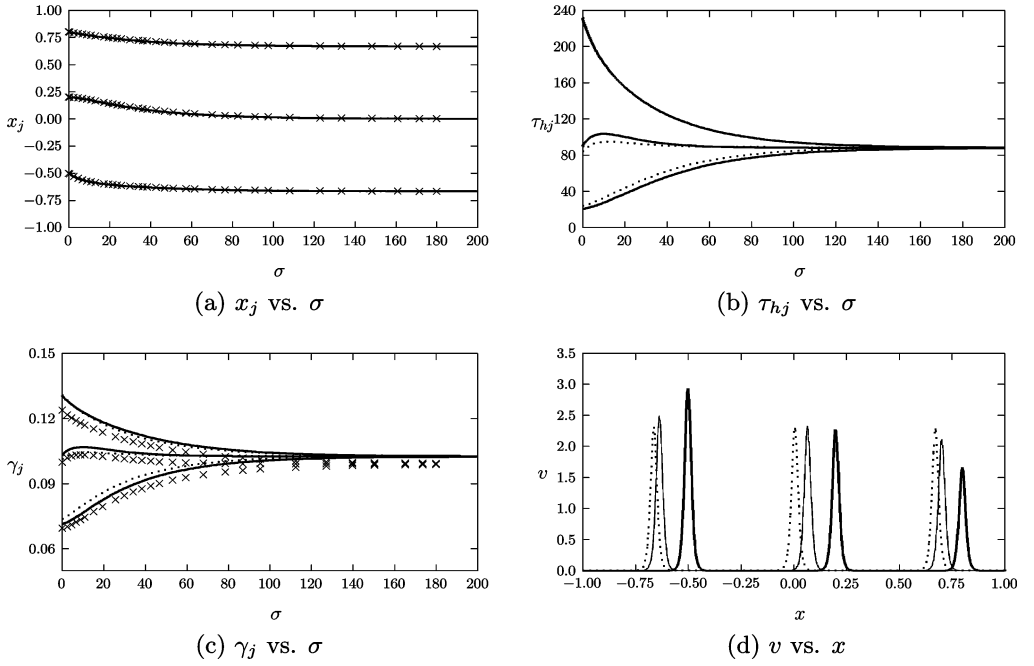
Next, we consider a three-spike evolution with parameter values $D = 1.0$, $\mathcal{A} = 10.0$, $\tau = 2.0$ and $\varepsilon = 0.005$. The initial spike locations are $x_1(0) = -0.50$, $x_2(0) = 0.20$ and $x_3(0) = 0.80$. In Figure 3(a) an Figure 3(c) we plot the the spike layer trajectories and spike amplitudes, respectively, computed from (2.25) and the two-term approximation (2.18). Snapshots of the quasi-equilibrium solution are shown in Figure 3(d). In Figure 3(b) we plot the three Hopf bifurcation values τ_{hj}, for $j = 1, \ldots, 3$, versus σ calculated from (3.20). In the plots of τ_{hj}, γ_j and x_j versus σ the solid curves correspond to computing the spike amplitudes from the nonlinear algebraic system (2.17), while the dotted curves correspond to the two-term approximation (2.18). In the plots of x_j and γ_j the marked points are the full numerical results computed from (1.1) using the software of [4]. As in Experiment 3.1, the asymptotic and full numerical results agree rather closely.

From Figure 2(a) we observe that the stability threshold $\tau_h(\sigma) \equiv \min_{j=1,2,3}[\tau_{hj}(\sigma)]$ is an increasing function of σ with $\tau_h(0) \approx 2.6$ and $\tau_h(\infty) \approx 14.0$. This monotonicity of $\tau_h(\sigma)$, together with $\tau_h(0) > \tau = 2.0$, again precludes the existence of a dynamically triggered Hopf bifurcation in the spike amplitudes.

4 Oscillatory drift instabilities of k-spike patterns

In this section we compute numerical solutions to the Stefan problem (2.12) when $\tau\varepsilon^2\mathcal{A}^2 = O(1)$ and $O(\varepsilon^{-1/3}) \ll \mathcal{A} \ll O(\varepsilon^{-1/2})$. For notational convenience, so as not to confuse spike locations with grid points of the discretization, we re-label the spike trajectories as $\xi_j(\sigma)$, for $j = 1, \ldots, k$. Then, defining $\tau_0 \equiv \varepsilon^{-2}\mathcal{A}^{-2}\tau = O(1)$ to be the key

https://doi.org/10.1017/S0956792508007766 Published online by Cambridge University Press



(a) x_j vs. σ (b) τ_{hj} vs. σ

(c) γ_j vs. σ (d) v vs. x

FIGURE 3. *Experiment 3.2:* Slow evolution of a three-spike quasi-equilibrium solution for $\varepsilon = 0.005$, $\mathcal{A} = 10$ and $D = 1.0$, with $x_1(0) = -0.5$, $x_2(0) = 0.2$ and $x_3(0) = 0.80$, obtained from the two-term asymptotic result (2.18) for the spike amplitudes. Top Left: x_j versus σ. Top Right: τ_{hj} versus σ. Bottom Left: γ_j versus σ. Bottom Right: v versus x at $\sigma = 0$ (heavy solid curve), $\sigma = 40$ (solid curve) and $\sigma = 140$. Except for the plot of v versus x, the solid curves correspond to computing the spike amplitudes from (2.17), while the dotted curves correspond to the two-term approximation (2.18). The crosses in the plots of x_j and γ_j versus σ are the full numerical results computed from (1.1).

bifurcation parameter, (2.12) becomes

$$\tau_0 u_\sigma = D u_{xx} + (1-u) - \sum_{j=1}^{k} 6\gamma_j \, \delta(x-\xi_j), \quad |x| \leqslant 1\,; \qquad u_x(\pm 1,\sigma) = 0, \tag{4.1a}$$

$$\xi_j' = \gamma_j [u_x(\xi_j^+,\sigma) + u_x(\xi_j^-,\sigma)], \qquad j = 1,\ldots,k, \tag{4.1b}$$

$$u(\xi_j(\sigma),\sigma) = 1/(\gamma_j \mathcal{A}^2), \qquad j = 1,\ldots,k. \tag{4.1c}$$

By using a SLEP approach, which is related to the method pioneered in [31], it was shown in [24] that a one-spike equilibrium solution will become unstable at some critical value of τ_0 to an oscillatory drift instability associated with a pure imaginary small eigenvalue $\lambda \ll 1$ of the linearization. As τ_0 increases above this critical value a complex conjugate pair of eigenvalues crosses into the right half-plane $\mathrm{Re}(\lambda) > 0$, leading to the initiation of a small-scale oscillatory motion of the spike location. This oscillatory drift

https://doi.org/10.1017/S0956792508007766 Published online by Cambridge University Press

instability is the dominant instability mechanism in the sub-regime $O(\epsilon^{-1/3}) \ll \mathcal{A} \ll O(\epsilon^{-1/2})$ of the intermediate regime.

For the one-spike case where $k = 1$, we now show that the condition for the stability of the equilibrium solution to the Stefan problem (4.1) is equivalent to that obtained in [24] using the SLEP method. We let $U \equiv U(x)$ and $\gamma_1 = \gamma_{1e}$ denote the equilibrium solution to (4.1) with $\xi_1 = 0$. Then,

$$DU_{xx} + (1 - U) = 0, \quad |x| < 1; \quad U_x(\pm 1) = 0; \quad [DU_x]_0 = 6\gamma_{1e}; \quad U(0) = \frac{1}{\gamma_e \mathcal{A}^2}. \tag{4.2}$$

Here we have defined $[v]_0 \equiv v(0^+) - v(0^-)$. We readily calculate that

$$U = 1 - B\frac{\cosh(\theta_0(1+x))}{\cosh\theta_0}, \quad -1 \leqslant x < 0; \qquad U = 1 - B\frac{\cosh(\theta_0(1-x))}{\cosh\theta_0}, \quad 0 < x \leqslant 1, \tag{4.3a}$$

where $\theta_0 \equiv D^{-1/2}$, and

$$\gamma_{1e} \equiv \frac{B\sqrt{D}}{3}\tanh\theta_0, \qquad B \equiv 1 - \frac{1}{\gamma_{1e}\mathcal{A}^2}. \tag{4.3b}$$

By solving the quadratic equation for γ_{1e} we get

$$\gamma_{1e} = \frac{\sqrt{D}}{6}\tanh\theta_0\left[1 + \sqrt{1 - \frac{\mathcal{A}_{1e}^2}{\mathcal{A}^2}}\right], \qquad \mathcal{A}_{1e} \equiv \sqrt{\frac{12\theta_0}{\tanh\theta_0}}. \tag{4.3c}$$

For $\mathcal{A} \gg 1$, we readily obtain that

$$\gamma_{1e} = \frac{\sqrt{D}}{3}\tanh\theta_0 - \frac{1}{\mathcal{A}^2} + O(\mathcal{A}^{-4}), \qquad B = 1 - \frac{3}{\mathcal{A}^2\sqrt{D}\tanh\theta_0} + O(\mathcal{A}^{-4}). \tag{4.3d}$$

For $\delta \ll 1$, we perturb the equilibrium solution as

$$u(x,\sigma) = U(x) + \delta e^{\lambda\sigma}\phi(x), \qquad \gamma_1 = \gamma_{1e} + \delta\beta e^{\lambda\sigma}, \qquad \xi_1 = \delta e^{\lambda\sigma}. \tag{4.4}$$

We substitute (4.4) into (4.1a), and collect $O(\delta)$ terms to get $D\phi_{xx} - (1 + \tau_0\lambda)\phi = 0$ on $|x| \leqslant 1$. From the linearization of the ODE (4.1b), we obtain

$$\delta\lambda e^{\lambda\sigma} = (\gamma_{1e} + \delta\beta e^{\lambda\sigma})(U_x(0^+) + U_x(0^-) + \delta e^{\lambda\sigma}[\phi_x(0^+) + \phi_x(0^-) + U_{xx}(0^+) + U_{xx}(0^-)]). \tag{4.5a}$$

In addition, the conditions $[Du_x]_{\xi_1} = 6\gamma_1$ and $u(\xi_1) = 1/(\gamma_1\mathcal{A}^2)$ become

$$D(U_x(0^+) - U_x(0^-) + \delta e^{\lambda\sigma}[U_{xx}(0^+) - U_{xx}(0^+) + \phi_x(0^+) - \phi_x(0^-)]) = 6(\gamma_{1e} + \varepsilon\delta e^{\lambda\sigma}), \tag{4.5b}$$

$$U(0^\pm) + \delta e^{\lambda t}(U_x(0^\pm) + \phi(0^\pm)) = \frac{1}{\gamma_{1e}\mathcal{A}^2} - \frac{\delta\beta}{\gamma_{1e}^2\mathcal{A}^2}e^{\lambda\sigma}. \tag{4.5c}$$

https://doi.org/10.1017/S0956792508007766 Published online by Cambridge University Press

Since $U_x(0^+) + U_x(0^-) = 0$, $U_{xx}(0^+) = U_{xx}(0^-)$, and $U_x(0^+) = \pm 3\gamma_{1e}/D$, we collect the $O(\delta)$ terms in (4.5) to obtain the following problem for ϕ:

$$D\phi_{xx} - (1 + \tau_0\lambda)\,\phi = 0, \quad |x| \leqslant 1\,; \quad \phi_x(\pm 1) = 0, \tag{4.6a}$$

$$[D\phi_x]_0 = 6\beta\,; \qquad \phi(0^{\pm}) = \mp\frac{3\gamma_{1e}}{D} - \frac{\beta}{\gamma_{1e}^2\mathcal{A}^2}, \tag{4.6b}$$

$$\lambda = 2\gamma_{1e}\left(U_{xx}(0) + \frac{1}{2}[\phi_x(0^+) + \phi_x(0^-)]\right). \tag{4.6c}$$

The solution to (4.6a) satisfying the prescribed values for $\phi(0^{\pm})$ is

$$\phi = C_-\frac{\cosh(\theta_\lambda(x+1))}{\cosh\theta_\lambda}, \quad -1 \leqslant x < 0\,; \qquad u = C_+\frac{\cosh(\theta_\lambda(1-x))}{\cosh\theta_\lambda}, \quad 0 < x \leqslant 1, \tag{4.7a}$$

where $\theta_\lambda \equiv \theta_0\sqrt{1+\tau_0\lambda}$, and

$$C_\pm = \mp\frac{3\gamma_{1e}}{D} - \frac{\beta}{\gamma_{1e}^2\mathcal{A}^2}. \tag{4.8}$$

The jump condition $[D\phi_x]_0 = 6\beta$, then yields that $\beta = 0$. Then, we substitute values for $\phi_x(0^{\pm})$ and $U_{xx}(0) = -D^{-1}(1 - 1/(\gamma_{1e}\mathcal{A}^2))$ into (4.6c) to obtain

$$\lambda = 2\gamma_{1e}\left[\frac{3\gamma_{1e}}{D}\theta_\lambda\tanh\theta_\lambda - \frac{1}{D}\left(1 - \frac{1}{\gamma_{1e}\mathcal{A}^2}\right)\right]. \tag{4.9}$$

Finally, by using (4.3c) for γ_{1e}, we readily derive that λ satisfies the transcendental equation

$$\lambda = \mu[\sqrt{1+\tau_0\lambda}\tanh\theta_0\tanh\theta_\lambda - 1], \qquad \mu \equiv \frac{\theta_0}{6}\tanh\theta_0\left[1 + \sqrt{1 - \frac{\mathcal{A}_{1e}^2}{\mathcal{A}^2}}\right]^2. \tag{4.10}$$

Here $\theta_\lambda \equiv \theta_0\sqrt{1+\tau_0\lambda}$, $\theta_0 \equiv D^{-1/2}$, while $\mathcal{A}_{1e}$ is defined in (4.3c). Equation (4.10) is identical to that derived in (5.5) of [24] from using the SLEP method based on a linearization of (1.1) around a one-spike equilibrium solution.

We introduce ω, τ_d, and ζ, by $\lambda = \mu\omega$, $\tau_0 = \tau_d/\mu$, and $\zeta = \tau_d\omega$. Then, from (4.10), ζ is a root of

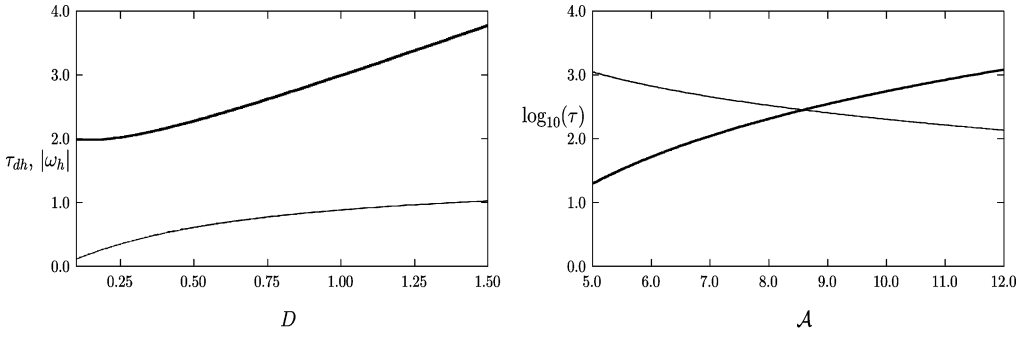
$$F(\zeta) \equiv \frac{\zeta}{\tau_d} - G(\zeta) = 0, \qquad G(\zeta) \equiv \sqrt{1+\zeta}\tanh\theta_0\tanh[\theta_0\sqrt{1+\zeta}] - 1. \tag{4.11}$$

By examining the roots of (4.11) in the complex ζ plane, the following result was proved in Section 5 of [24].

Proposition 4.1 *There is a complex conjugate pair of pure imaginary eigenvalues to (4.10) at some unique value $\tau_d = \tau_{dh}$ depending on D. For any $\tau_d > \tau_{dh}$ there are exactly two eigenvalues in the right half-plane. These eigenvalues have nonzero imaginary parts when $\tau_{dh} < \tau_d < \tau_{dm}$, and they merge onto the positive real axis at $\tau_d = \tau_{dm}$. They remain on the positive real axis for all $\tau_d > \tau_{dm}$.*

The numerically computed Hopf bifurcation value τ_{dh} is plotted versus D in Figure 4(a). In Figure 4(a) we also plot the magnitude $|\omega_h|$ of the pure imaginary eigenvalues

https://doi.org/10.1017/S0956792508007766 Published online by Cambridge University Press



(a) τ_{dh} and $|\omega_h|$ vs. D (b) $\log_{10}(\tau_{tw})$ and $\log_{10}(\tau_h)$ vs. $\mathcal{A}$

FIGURE 4. Left Figure: The drift instability thresholds τ_{dh} (heavy solid curve) and $|\omega_h|$ (solid curve) versus D. Right figure: Plots of $\log_{10}(\tau_h)$ (heavy solid curve) from (3.21) with $k = 1$ and $\log_{10}(\tau_{tw})$ (solid curve) from (4.12) versus $\mathcal{A}$ for $D = 0.75$ and $\varepsilon = 0.015$. This shows the exchange in the dominant instability mechanism in the intermediate regime.

$\omega_h = \pm i|\omega_h|$ at $\tau_d = \tau_{dh}$. Since $\tau_0 = \tau_d/\mu$ and $\tau = \varepsilon^{-2}\mathcal{A}^{-2}\tau_0$, the Hopf bifurcation value for the onset of an oscillatory drift instability for a one-spike solution is

$$\tau_{tw} \sim \varepsilon^{-2}\mathcal{A}^{-2}\tau_{0d}, \qquad \tau_{0d} \equiv \frac{\tau_{dh}}{\mu}, \qquad \mu \equiv \frac{\theta_0}{6}\tanh\theta_0\left[1+\sqrt{1-\frac{\mathcal{A}_{1e}^2}{\mathcal{A}^2}}\right]^2. \tag{4.12}$$

Recall from (3.21) that there is an oscillatory instability in the amplitude of an equilibrium spike when $\tau = \tau_h = O(\mathcal{A}^4)$. Thus, $\tau_h \ll \tau_{tw}$ when $O(1) \ll \mathcal{A} \ll O(\varepsilon^{-1/3})$ and $\tau_{tw} \ll \tau_h$ when $O(\varepsilon^{-1/3}) \ll \mathcal{A} \ll O(\varepsilon^{-1/2})$. In Figure 4 we plot $\log_{10}(\tau_{tw})$ and $\log_{10}(\tau_h)$ versus $\mathcal{A}$, showing the exchange in the dominant instability mechanism in the intermediate regime. For the equilibrium problem on the infinite line this exchange in the dominant instability mechanism was also noted in [9, 27]. As a remark, we notice that ω_h, representing the (scaled) temporal frequency of small oscillations, satisfies $\omega_h \to 0$ in the infinitely long domain limit $D \to 0$. Therefore, the existence of an oscillatory instability requires a finite domain.

4.1 Numerical solution of the coupled ODE–PDE Stefan problem

To compute numerical solutions to the Stefan problem (4.1) we adapt the numerical method of [40] for computing solutions to a heat equation with a moving singular Dirac source term. We use a Crank–Nicolson scheme to discretize (4.1a) together with a forward Euler scheme for the ODE (4.1b).

For simplicity, we first consider (4.1a) for one spike where $k = 1$. Let h and Δt denote the space step and time step, respectively. We set $\Delta t = h^2/2$ to satisfy the stability requirement of the forward Euler scheme. The number of grid points is $M = 1 + 2/h$, and we label the jth grid point by $x_j = -1 + (j-1)h$ for $j = 1, \ldots, M$. The total time period is T_m, and we label $\sigma_n = n\Delta t$ for $n = 1, \ldots, T_m/\Delta t$. At time σ_n, the solution $u(x_j, \sigma_n)$ at the jth grid point is approximated by U_j^n, and we label $\mathbf{U}^n = (U_1^n, \cdots, U_M^n)^T$. Also, the spike location $\xi_1(\sigma_n)$ and spike amplitude $\gamma_1(\sigma_n)$ are approximated by ξ_1^n and γ_1^n, respectively.

https://doi.org/10.1017/S0956792508007766 Published online by Cambridge University Press

As in [40], we approximate the delta function $\delta(x-\xi_1)$ in (4.1a) with the discrete delta function $d^{(1)}(x-\xi_1)$, where $d^{(1)}(y)$ is given by

$$d^{(1)}(y)=\begin{cases}(2h-|y|)/(4h^2), & |y|\leqslant 2h,\\ 0, & \text{otherwise.}\end{cases} \tag{4.13}$$

The numerical approximation $d^{(1)}$ of the delta function in (4.1a) spreads the singular force to the neighbouring grid points within its support. Next, we write the constraint of (4.1c), given by $u(\xi_1(\sigma),\sigma)=1/(\gamma_1\mathcal{A}^2)$, in the form

$$u(\xi_1(\sigma),\sigma)=\int_{-\infty}^{\infty}u(x,\sigma)\delta(x-\xi_1(\sigma))\,\mathrm{d}x=\frac{1}{\gamma_1\mathcal{A}^2}. \tag{4.14}$$

With $U_j^n\approx u(x_j,\sigma_n)$, $\xi_1^n\approx\xi_1(\sigma_n)$ and $\gamma_1^n\approx\gamma_1(\sigma_n)$, the discrete version of (4.14) is

$$u(\xi_1^n,\sigma_n)\approx h\sum_j U_j^n d^{(2)}\big(x_j-\xi_1^n\big)=\frac{1}{\gamma_1^n\mathcal{A}^2}, \tag{4.15}$$

where $d^{(2)}(y)$ is a further numerical approximation to the delta function given explicitly by

$$d^{(2)}(y)=\frac{1}{h}\begin{cases}1-(y/h)^2, & |y|\leqslant h,\\ 2-3|y|/h+(y/h)^2, & h\leqslant|y|\leqslant 2h,\\ 0, & \text{otherwise.}\end{cases} \tag{4.16}$$

The function $d^{(2)}$ interpolates grid values U_j^n to approximate the requirement $u(\xi_1^n,\sigma_n)=1/(\gamma_1^n\mathcal{A}^2)$ at the spike location. A rough outline of the algorithm for the numerical solution to (4.1) to advance from the nth to the $(n+1)$th time-step is as follows: We first use (4.1b) to take a forward Euler step to get the new location ξ_1^{n+1} given $\mathbf{U}^n$ and γ_1^n. Then, we use the approximate condition

$$u\big(\xi_1^{n+1},\sigma_{n+1}\big)\approx\frac{1}{2\mathcal{A}^2}\left(\frac{1}{\gamma_1^n}+\frac{1}{\gamma_1^{n+1}}\right), \tag{4.17}$$

on the right-hand side of (4.15) together with the Crank–Nicolson discretization of (4.1a) to solve for γ_1^{n+1}. Then, we calculate $\mathbf{U}^{n+1}$ from the discretization of (4.1a) using the value of γ_1^{n+1}. Finally, we set $n=n+1$, and repeat the iteration.

In order to obtain higher accuracy, we use a fourth order accurate scheme as suggested in [40] to approximate the second order differential operator u_{xx} as

$$u_{xx}(x_j,\sigma_n)\approx\begin{cases}\big(U_{j+4}^n-6U_{j+3}^n+14U_{j+2}^n-4U_{j+1}^n-15U_j^n+10U_{j-1}^n\big)/(12h^2), & j=1,\\ \big(-U_{j+2}^n+16U_{j+1}^n-30U_j^n+16U_{j-1}^n-U_{j-2}^n\big)/(12h^2), & 2\leqslant j\leqslant N,\\ \big(U_{j-4}^n-6U_{j-3}^n+14U_{j-2}^n-4U_{j-1}^n-15U_j^n+10U_{j+1}^n\big)/(12h^2), & j=M,\end{cases}$$

where U_0^n and U_{M+1}^n are ghost points outside each end of the boundaries at $x=\pm1$. The Neumann condition $u_x(\pm1,t)=0$ is also discretized as

$$u_x(x_1,\sigma_n)\approx\big(-3U_0^n-10U_1^n+18U_2^n-6U_3^n+U_4^n\big)/(12h),$$
$$u_x(x_M,\sigma_n)\approx\big(3U_{M+1}^n+10U_M^n-18U_{M-1}^n+6U_{M-2}^n-U_{M-3}^n\big)/(12h).$$

https://doi.org/10.1017/S0956792508007766 Published online by Cambridge University Press

Eliminating the ghost points from the discretization of u_{xx}, we obtain the $M \times M$ coefficient matrix

$$\mathbf{T} = \frac{1}{12h^2}\begin{pmatrix} -145/3 & 56 & -6 & -8/3 & 1 & 0 & 0 & 0 & \cdots & 0 \\ 58/3 & -36 & 18 & -4/3 & 0 & 0 & 0 & 0 & \cdots & 0 \\ -1 & 16 & -30 & 16 & -1 & 0 & 0 & 0 & \cdots & 0 \\ 0 & -1 & 16 & -30 & 16 & -1 & 0 & 0 & \cdots & 0 \\ 0 & 0 & -1 & 16 & -30 & 16 & -1 & 0 & \cdots & 0 \\ & & & \ddots & \ddots & \ddots & \ddots & \ddots & & \\ 0 & \cdots & 0 & 0 & -1 & 16 & -30 & 16 & -1 & 0 \\ 0 & \cdots & 0 & 0 & 0 & -1 & 16 & -30 & 16 & -1 \\ 0 & \cdots & 0 & 0 & 0 & 0 & -4/3 & 18 & -36 & 58/3 \\ 0 & \cdots & 0 & 0 & 0 & 1 & -8/3 & -6 & 56 & -145/3 \end{pmatrix}.$$

Next, we outline how we calculate the fluxes in (4.1b). For convenience, in the notation of this paragraph we omit the superscript n at time σ_n. In order to approximate the one-sided first order derivatives $u_x(\xi_1^{\pm}, \sigma_n)$ in (4.1b), we first use the solution values at grid points on each side of ξ_1 to interpolate the values at points that are equally distributed near ξ_1. Then, we approximate $u_x(\xi_1^{\pm}, \sigma_n)$ by differencing values at these points. For instance, assuming that the closest grid point on the left-hand side of the spike is x_j, we use six point values $(\bar{u}, U_j, U_{j-1}, U_{j-2}, U_{j-3}, U_{j-4})$ with $\bar{u} = u(\xi_1, \sigma_n) = 1/(\gamma_1 \mathcal{A}^2)$ to interpolate the solution at $x = (\xi_1 - 3h, \xi_1 - 2h, \xi_1 - h, \xi_1)$. Denoting the results to be $(U_1^-, U_2^-, U_3^-, U_4^-)$ with $U_4^- = u(\xi_1, \sigma_n) = 1/(\gamma_1 \mathcal{A}^2)$, we can use them for estimating $u_x(\xi_1^-, \sigma_n)$ as

$$u_x(\xi_1^-, t) \approx \left(-3U_3^- + \frac{3}{2}U_2^- - \frac{1}{3}U_1^- \right)/h. \tag{4.18a}$$

Similarly, we obtain $(U_1^+, U_2^+, U_3^+, U_4^+)$ at $x = (\xi_1, \xi_1 + h, \xi_1 + 2h, \xi_1 + 3h)$ by interpolation, and we then discretize to obtain

$$u_x(\xi_1^+, t) \approx \left(3U_2^+ - \frac{3}{2}U_3^+ + \frac{1}{3}U_4^+ \right)/h. \tag{4.18b}$$

Next, we discretize (4.1a) by the Crank–Nicolson scheme to get

$$\left[\left(1 + \frac{1}{2}\mu\right)\mathbf{I} - \frac{\mu D}{2}\mathbf{T} \right] \mathbf{U}^{n+1} = \left[\left(1 - \frac{1}{2}\mu\right)\mathbf{I} + \frac{\mu D}{2}\mathbf{T} \right] \mathbf{U}^n - 3\mu \left(\mathbf{d}^{n+1}\gamma_1^{n+1} + \mathbf{d}^n \gamma_1^n \right) + \mathbf{p}, \tag{4.19}$$

where $\mu \equiv \Delta t/\tau_0$ and $\mathbf{p}^t \equiv (\mu, \mu, \ldots, \mu)$. Here $\mathbf{d}^{n+1}$ denotes the discretization of the delta function by $d^{(1)}$ at time σ_{n+1}. Denoting the coefficient matrix of $\mathbf{U}^{n+1}$ to be $\mathbf{A}$ and that of $\mathbf{U}^n$ to be $\mathbf{B}$, the system above can be written in the simpler form

$$\mathbf{A}\mathbf{U}^{n+1} = \mathbf{B}\mathbf{U}^n - 3\mu \left(\mathbf{d}^{n+1}\gamma_1^{n+1} + \mathbf{d}^n \gamma_1^n \right) + \mathbf{p}. \tag{4.20}$$

https://doi.org/10.1017/S0956792508007766 Published online by Cambridge University Press

In (4.20), only the boldface variables are matrices and vectors. We then approximate (4.1c) by the discrete form (4.15). We write this interpolation as a dot product $\mathbf{N}^{n+1}\mathbf{U}^{n+1}$, where

$$\mathbf{N}^{n+1}\mathbf{U}^{n+1} = \frac{1}{2\mathcal{A}^2}\left(\frac{1}{\gamma_1^n} + \frac{1}{\gamma_1^{n+1}}\right). \tag{4.21}$$

Since $\mathbf{A}$ has full rank, we then left multiply (4.20) by $\mathbf{N}^{n+1}\mathbf{A}^{-1}$ to get a quadratic equation for γ_1^{n+1} given by

$$3\mu\mathbf{N}^{n+1}\mathbf{A}^{-1}\mathbf{d}^{n+1}\gamma_1^{n+1} - \left[\mathbf{N}^{n+1}\mathbf{A}^{-1}(\mathbf{B}\mathbf{U}^n - 3\mu\mathbf{d}^n\gamma_1^n + \mathbf{p}) - \frac{1}{2\mathcal{A}^2}\frac{1}{\gamma_1^n}\right] + \frac{1}{2\mathcal{A}^2}\frac{1}{\gamma_1^{n+1}} = 0. \tag{4.22}$$

Since $\mathcal{A} \gg 1$, we can solve (4.22) for the correct root γ_1^{n+1}. We then calculate $\mathbf{U}^{n+1}$ using (4.20) and start the next iteration by using a forward Euler step on (4.1b) to advance the spike location.

This numerical method can be readily extended to treat (4.1) for two or more spikes. For instance, consider the case of two spikes. With the same Crank–Nicolson scheme, we let $\mathbf{d}_1$ and $\mathbf{d}_2$ be the discrete approximations of $\delta(x-\xi_1)$ and $\delta(x-\xi_2)$ in (4.1a), respectively, with the discrete delta function $d^{(1)}$. Define the row vectors $\mathbf{N}_1^{n+1}$ and $\mathbf{N}_2^{n+1}$ to the discrete versions of $d^{(2)}$ near ξ_1 and ξ_2, respectively. The conditions $u(\xi_j^{n+1}, \sigma^{n+1}) = 1/(\gamma_j^{n+1}\mathcal{A}^2)$, can then be approximated by the two discrete constraints

$$\mathbf{N}_j^{n+1}\mathbf{U}^{n+1} = \frac{1}{2\mathcal{A}^2}\left(\frac{1}{\gamma_j^n} + \frac{1}{\gamma_j^{n+1}}\right), \quad \text{for} \quad j = 1, 2. \tag{4.23}$$

The Crank–Nicolson discretization of (4.1a) with $k = 2$ is written as

$$\mathbf{A}\mathbf{U}^{n+1} = \mathbf{B}\mathbf{U}^n - 3\mu\left(\mathbf{d}_1^{n+1}\gamma_1^{n+1} + \mathbf{d}_2^{n+1}\gamma_2^{n+1}\right) - 3\mu\left(\mathbf{d}_1^n\gamma_1^n + \mathbf{d}_2^n\gamma_2^n\right) + \mathbf{p}. \tag{4.24}$$

Upon imposing the constraints (4.23) we obtain the following system for γ_1^{n+1} and γ_2^{n+1}:

$$\begin{aligned} &3\mu\mathbf{N}_j^{n+1}\mathbf{A}^{-1}\left(\mathbf{d}_1^{n+1}\gamma_1^{n+1} + \mathbf{d}_2^{n+1}\gamma_2^{n+1}\right) + \frac{1}{2\mathcal{A}^2}\frac{1}{\gamma_j^{n+1}} \\ &\quad - \left[\mathbf{N}_j^{n+1}\mathbf{A}^{-1}\left(\mathbf{B}\mathbf{U}^n - 3\mu\left(\mathbf{d}_1^n\gamma_1^n + \mathbf{d}_2^n\gamma_2^n\right) + \mathbf{p}\right) - \frac{1}{2\mathcal{A}^2}\frac{1}{\gamma_j^n}\right] = 0, \quad \text{for} \quad j = 1, 2. \end{aligned} \tag{4.25}$$

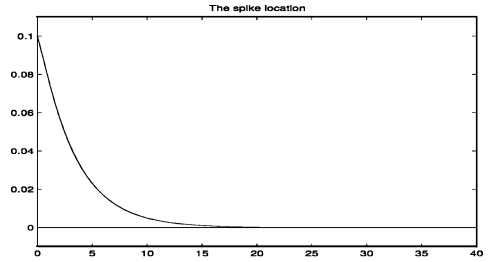
After calculating γ_1^{n+1} and γ_2^{n+1} from this system, we then compute $\mathbf{U}^{n+1}$ from (4.25), and update the locations of the spikes.

4.2 Numerical experiments of oscillatory drift instabilities

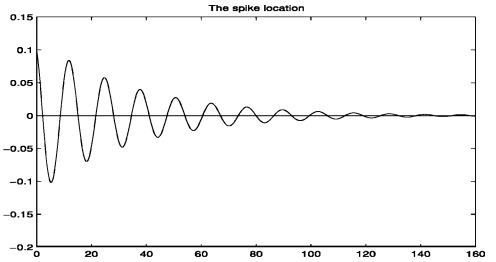
We now perform some numerical experiments on (4.1) to verify the drift instability threshold of a one-spike solution given in (4.12). We also use the numerical scheme of Section 4.1 to compute large-scale oscillatory motion for some one and two-spike patterns.

For each of the numerical experiments below we give initial spike locations $\xi_j(0) = \xi_{j0}$, for $j = 1, \ldots, k$, and we choose the initial condition $u(x, 0)$ for (4.1) to be the quasi-equilibrium solution (2.13) with $g_j = 1$ and $x_j = \xi_{j0}$ for $j = 1, \ldots, k$ in (2.13). In

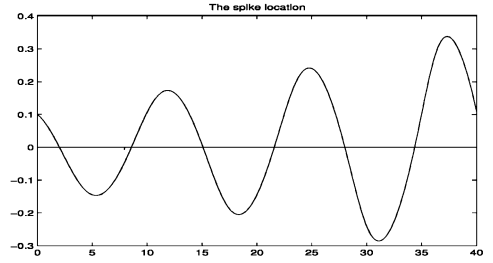
https://doi.org/10.1017/S0956792508007766 Published online by Cambridge University Press



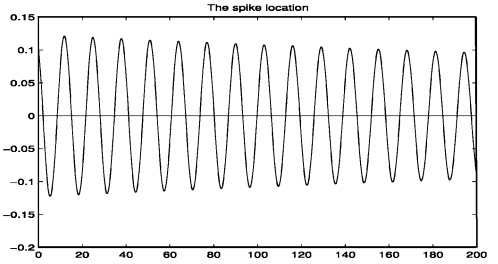
(a) ξ_1 vs. σ for $\tau_0 = 1.0$



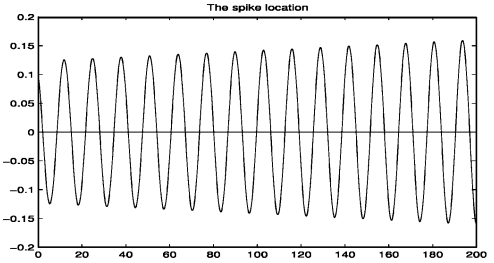
(b) ξ_1 vs. σ for $\tau_0 = 4.0$



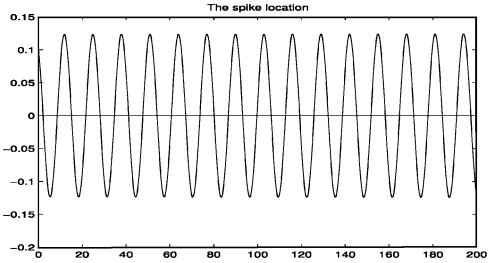
(c) ξ_1 vs. σ for $\tau_0 = 4.4$



(d) ξ_1 vs. σ for $\tau_0 = 4.20$



(e) ξ_1 vs. σ for $\tau_0 = 4.22$



(f) ξ_1 vs. σ for $\tau_0 = 4.21$

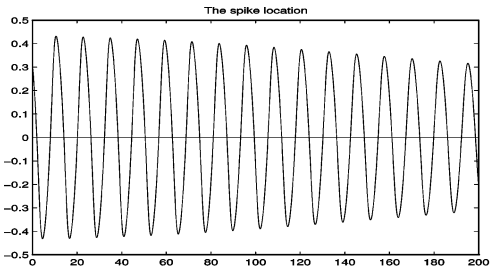
FIGURE 5. *Experiment 4.1:* Testing the stability threshold for initial values near the equilibrium value. Plots of ξ_1 versus σ with $\xi_1(0) = 0.1$, $D = 0.75$ and $\mathcal{A} = 28.5$, for different values of τ_0. The numerical threshold $\tau_{0d} \approx 4.21$ in the plot in the lower right figure compares well with the theoretical prediction $\tau_{0d} \approx 4.19$.

all of the numerical computations below, we chose the mesh size $h = 0.01$ and the diffusivity $D = 0.75$. For $D = 0.75$, the stability threshold from Proposition 4.1 is computed numerically as $\tau_{dh} = 2.617$.

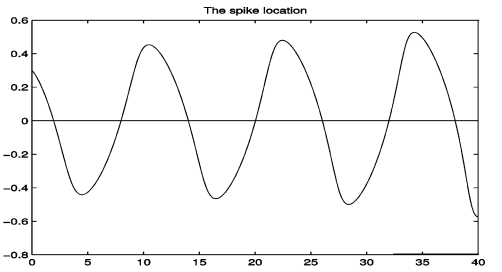
Experiment 4.1: A one-spike solution near equilibrium: Testing the instability threshold

Let $D = 0.75$ and $\mathcal{A} = 28.5$. Then, from (4.12) we calculate $\tau_{0d} \approx 4.19$. For an initial spike location at $\xi_1(0) = 0.1$, in Figure 5 we plot the numerically computed spike layer trajectory ξ_1 versus σ for six values of τ_0. Comparing Figure 5(d) with Figure 5(e), we see that the amplitude of the oscillation grows slowly when $\tau_0 = 4.22$, and decays slowly when $\tau_0 = 4.20$. From Figure 5(f) we observe that the drift Hopf bifurcation value is

https://doi.org/10.1017/S0956792508007766 Published online by Cambridge University Press



(a) ξ_1 vs. σ for $\tau_0 = 4.20$



(b) ξ_1 vs. σ for $\tau_0 = 4.22$

FIGURE 6. *Experiment 4.2:* Plots of ξ_1 versus σ with $\xi_1(0) = 0.3$, $D = 0.75$ and $\mathcal{A} = 28.5$. Left figure: $\tau_0 = 4.20$. Right figure: $\tau_0 = 4.22$.

$\tau_{0d} \approx 4.21$, which compares favourably with the theoretical prediction of $\tau_{0d} \approx 4.19$ from (4.12). With regards to the convergence of the numerical scheme for (4.1), we estimate numerically that $\tau_{0d} \approx 4.23$ with the coarser mesh size $h = 0.02$, and that $\tau_{0d} \approx 4.20$ for the very fine mesh size $h = 0.005$. As a trade-off between accuracy and computational expense, we chose $h = 0.01$ in our computations.

Experiment 4.2: A one-spike solution: Large-scale oscillatory dynamics

We again let $D = 0.75$ and $\mathcal{A} = 28.5$. However, we now choose the initial spike location $\xi_1(0) = 0.3$, which is not near its equilibrium value. In Figure 6 we plot the numerically computed spike layer trajectory ξ_1 versus σ for $\tau_0 = 4.20$ and $\tau_0 = 4.22$. For the smaller value of τ_0 the spike slowly approaches its steady state at $\xi_1 = 0$. However, for $\tau_0 = 4.22$, the spike location exhibits a sustained large-scale oscillation.

Experiment 4.3: A two-spike pattern: Oscillatory drift instabilities and the breather mode

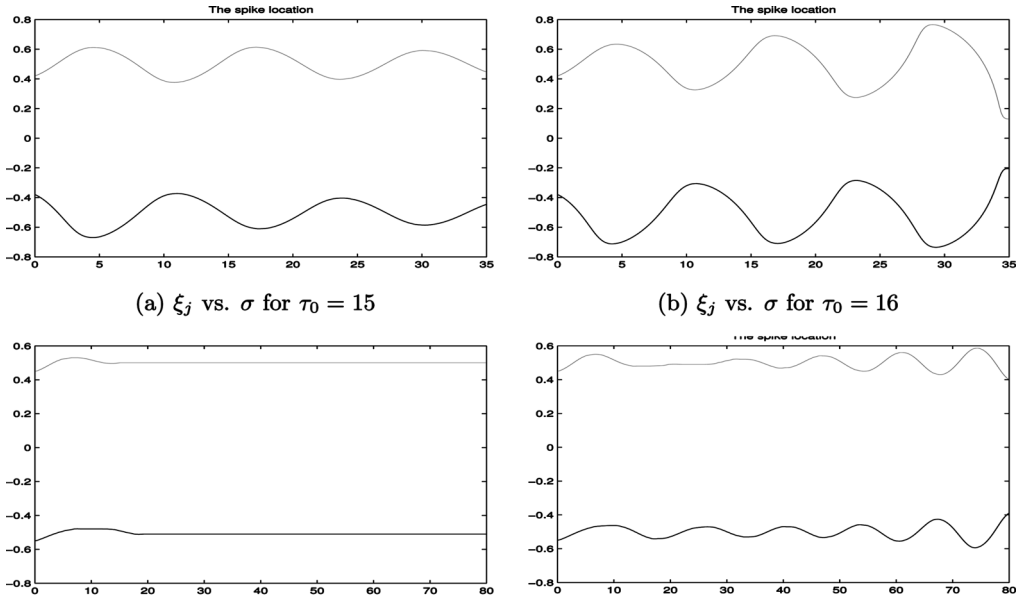
We now compute two-spike solutions. For $D = 0.75$ and $\mathcal{A} = 63.6$, in Figure 7(a) and Figure 7(b) we plot the numerically computed spike trajectories with initial values $\xi_1(0) = -0.38$ and $\xi_2(0) = 0.42$ for two values of τ_0. For $\tau_0 = 16$, the spike trajectories develop a large-scale sustained oscillatory motion. In each case, the observed oscillation is of breather type, characterized by a 180° out of phase oscillation in the spike locations. A breather instability was shown in [16] to be the dominant instability mode for instabilities of equilibrium transition layer patterns for a FitzHugh–Nagumo type model. It is also the dominant instability mode for equilibrium spike patterns of the GS model in the high-feed rate regime $\mathcal{A} = O(\varepsilon^{-1/2})$ (see [23]). For the same values of D and $\mathcal{A}$, in Figure 7(c) and Figure 7(d) we plot the numerically computed spike trajectories with initial values $\xi_1(0) = -0.55$ and $\xi_2(0) = 0.45$ for $\tau_0 = 15$ and $\tau_0 = 17$, respectively.

4.3 Integral equation formulation

In this section, we show how to cast the Stefan problem (4.1) for a one-spike solution into an equivalent integral equation formulation. We let $K(x, \sigma; \eta, s)$ to be the Green's function satisfying

$$\tau_0 K_\sigma = DK_{xx} - K + \delta(x - \eta)\delta(\sigma - s), \qquad -1 < x < 1; \qquad K_x = 0 \quad x = \pm 1, \quad (4.26)$$

https://doi.org/10.1017/S0956792508007766 Published online by Cambridge University Press



(a) ξ_j vs. σ for $\tau_0 = 15$ (b) ξ_j vs. σ for $\tau_0 = 16$

(c) ξ_j vs. σ for $\tau_0 = 15$ (d) ξ_j vs. σ for $\tau_0 = 17$

FIGURE 7. *Experiment 4.3:* Spike trajectories ξ_j versus σ for a two-spike pattern with $D = 0.75$ and $\mathcal{A} = 63.6$. Top row: the initial values $\xi_1(0) = -0.38$ and $\xi_2(0) = 0.42$ with $\tau_0 = 15$ and $\tau_0 = 16$. Bottom Row: the initial values $\xi_1(0) = -0.55$ and $\xi_2(0) = 0.45$ with $\tau_0 = 15$ and $\tau_0 = 17$.

where $K = 0$ for $0 < \sigma < s$. The solution to (4.26) is represented as an eigenfunction expansion as

$$K(x,\sigma;\eta,s) = \frac{H(\sigma-s)}{\tau_0} e^{-(\sigma-s)/\tau_0} \times \left[\frac{1}{2} + \sum_{n=1}^{\infty} \exp\left(-\frac{Dn^2\pi^2}{4}\frac{(\sigma-s)}{\tau_0}\right) \cos\left(\frac{n\pi}{2}(\xi+1)\right) \cos\left(\frac{n\pi}{2}(\eta+1)\right)\right]. \tag{4.27}$$

By using Green's identity, a straightforward calculation shows that the solution $u(x,\sigma)$ to (4.1) with one spike can be written in terms of K as

$$u(x,\sigma) = 1 + \tau_0 \int_{-1}^{1} [u(\eta,0) - 1]\, K(x,\sigma;\eta,0)\, \mathrm{d}\eta - 6 \int_0^{\sigma} \gamma_1(s) K(x,\sigma;\xi_1(s),s)\, \mathrm{d}s, \tag{4.28}$$

where $\xi_1(s)$ is the spike trajectory. By imposing the constraint condition $u = 1/(\gamma_1 \mathcal{A}^2)$ at $x = \xi_1(\sigma)$, we obtain an integral equation for $\gamma_1(\sigma)$ in terms of the unknown spike location as

$$\frac{1}{\gamma_1(\sigma)\mathcal{A}^2} = 1 + \tau_0 \int_{-1}^{1} [u(\eta,0) - 1]\, K(\xi_1(\sigma),\sigma;\eta,0)\, \mathrm{d}\eta - 6 \int_0^{\sigma} \gamma_1(s) K(\xi_1(\sigma),\sigma;\xi_1(s),s)\, \mathrm{d}s. \tag{4.29}$$

https://doi.org/10.1017/S0956792508007766 Published online by Cambridge University Press

Then, by calculating u_x as $x \to \xi_1(\sigma)$ from above and from below, we calculate

$$u_x(\xi_1^{\pm}(\sigma),\sigma) = \tau_0 \int_{-1}^{1} [u(\eta,0)-1]\, K_x(\xi_1^{\pm}(\sigma),\sigma;\eta,0)\,\mathrm{d}\eta - 6\int_0^{\sigma} \gamma_1(s) K_x(\xi_1^{\pm}(\sigma),\sigma;\xi_1(s),s)\,\mathrm{d}s. \tag{4.30}$$

Finally, by substituting (4.30) into (4.1c), we obtain the integrodifferential equation

$$\frac{\mathrm{d}\xi_1}{\mathrm{d}\sigma} = \gamma_1(\sigma)\left(\tau_0 \int_{-1}^{1} [u(\eta,0)-1]\,(K_x(\xi_1^{+}(\sigma),\sigma;\eta,0)+K_x(\xi_1^{-}(\sigma),\sigma;\eta,0))\,\mathrm{d}\eta \right.$$
$$\left. -6\int_0^{\sigma} \gamma_1(s)(K_x(\xi_1^{+}(\sigma),\sigma;\xi_1(s),s)+K_x(\xi_1^{-}(\sigma),\sigma;\xi_1(s),s))\,\mathrm{d}s.\right) \tag{4.31}$$

Here $u(\eta,0)$ is the initial condition for (4.1). This shows that the speed of the spike layer at time σ depends on its entire past history. Therefore, $\xi_1(\sigma)$ is determined, essentially, by a continuously distributed delay model. Such problems typically lead to oscillatory behaviour when τ_0 is large enough. This suggests the mechanism underlying the oscillatory dynamics computed in Section 4.2.

We remark that as a result of the infinite series representation of K in (4.27), together with the constraint (4.29) for γ_1, the integrodifferential equation (4.31) is significantly more complicated in form than a related integrodifferential equation modeling a flame-front on the infinite line that was studied numerically in [36].

5 Discussion

We have studied the dynamics and oscillatory instabilities of spike solutions to the one-dimensional GS model (1.1) in the intermediate regime $O(1) \ll \mathcal{A} \ll O(\varepsilon^{-1/2})$ of the feed-rate parameter $\mathcal{A}$. In the sub-regime $O(1) \ll \mathcal{A} \ll O(\varepsilon^{-1/3})$, and for $\tau \ll O(\varepsilon^{-2}\mathcal{A}^2)$, we have derived an explicit DAE system for the spike trajectories from the quasi-steady limit of the Stefan problem (2.12). From the analysis of a certain nonlocal eigenvalue problem, it was shown that the instantaneous spike pattern in this regime will become unstable to a Hopf bifurcation in the spike amplitudes at some critical value $\tau = \tau_H = O(\mathcal{A}^4)$. Alternatively, in the sub-regime $O(\epsilon^{-1/3}) \ll \mathcal{A} \ll O(\epsilon^{-1/2})$, and with $\tau = O(\varepsilon^{-2}\mathcal{A}^{-2})$, oscillatory drift instabilities for the spike locations were computed numerically from the full time-dependent Stefan problem (4.1) with moving sources. In this sub-regime, the onset of such drift instabilities occur at some critical value $\tau = \tau_{TW} = O(\varepsilon^{-2}\mathcal{A}^{-2})$ that can be calculated analytically. An open technical problem is to study the codimension two bifurcation problem that occurs when $\mathcal{A} = O(\varepsilon^{-1/3})$ where both types of oscillatory instability can occur simultaneously at some critical value of $\tau = O(\varepsilon^{-4/3})$.

There are two key open problems. The first problem is to extend the numerical approach of [36], used for a flame-front integrodifferential equation model, to compute long-time solutions to the integrodifferential equation formulation (4.31) of the Stefan problem (4.1). With such an approach, one could compute numerical solutions to (4.1) over very long time intervals to study whether irregular, or even chaotic, large-scale oscillatory drift behaviour of the spike trajectories is possible for the GS model in the sub-regime $O(\varepsilon^{-1/3}) \ll \mathcal{A} \ll O(\varepsilon^{-1/2})$. A second direction of inquiry is to derive Stefan-type problems with moving sources from an asymptotic reduction of related reaction–diffusion systems with localized solutions such as the Gierer-Meinhardt model with saturation [20], the

https://doi.org/10.1017/S0956792508007766 Published online by Cambridge University Press

combustion–reaction model of [26], the Brusselator model of [21] and the GS model in two spatial dimensions. The derivation of such Stefan problems would allow for the study of large-scale drift instabilities of localized structures for parameter values far from their bifurcation values at which a normal form reduction, such as in [13, 14], can be applied.

Acknowledgement

M.J.W. gratefully acknowledges the financial support of NSERC (Canada) under grant 81541.

References

[1] Astrov, Y. A. & Purwins, H. G. (2006) Spontaneous division of dissipate solitions in a planar gas-discharge with high ohmic electrode. *Phys. Lett. A* **358**(5–6), 404–408.

[2] Astrov, Y. A. & Purwins, H. G. (2001) Plasma spots in a gas discharge system: Birth, scattering and formation of molecules. *Phys. Lett. A* **283**(3–4), 349–354.

[3] Beyer, R. P. & Leveque, R. J. (1992) Analysis of a one-dimensional model for the immersed boundary method. *SIAM J. Numer. Anal.* **29**(2), 332–364.

[4] Blom, J. G. & Zegeling, P. A. (1994) Algorithm 731: A moving-grid interface for systems of one-dimensional time-dependent partial differential equations. *ACM Trans. Math. Software* **20**(2), 194–214.

[5] Bode, M., Liehr, A. W., Schenk, C. P. & Purwins, H. G. (2002) Interactions of dissipative solitons: Particle-like behaviour of localized structures in a three component reaction–diffusion system. *Physica D*(1–2) 45–66.

[6] Davis, P. W., Blanchedeau, P., Dullos, E. & De Kepper, P. (1998) Dividing blobs, chemical flowers, and patterned islands in a reaction–diffusion system. *J. Phys. Chem. A* **102**(43), 8236–8244.

[7] Doelman, A., Eckhaus, W. & Kaper, T. J. (2000) Slowly modulated two-pulse solutions in the Gray-Scott model I: Asymptotic construction and stability. *SIAM J. Appl. Math.* **61**(3), 1080–1102.

[8] Doelman, A., Eckhaus, W. & Kaper, T. J. (2000) Slowly modulated two-pulse solutions in the Gray-Scott model II: Geometric theory, bifurcations, and splitting dynamics. *SIAM J. Appl. Math.* **61**(6), 2036–2061.

[9] Doelman, A., Gardner, R. A. & Kaper, T. J. (1998) Stability analysis of singular patterns in the 1D Gray-Scott model: A matched asymptotics approach. *Physica D* **122**(1–4), 1–36.

[10] Doelman, A., Gardner, R. A. & Kaper, T. J. (2002) A stability index analysis of 1D patterns of the Gray-Scott model. *Memoirs of the AMS* **155**.

[11] Doelman, A. & Kaper, T. (2003) Semi-strong pulse interactions in a class of coupled reaction–diffusion equations. *SIAM J. Appl. Dyn. Sys.* **2**(1), 53–96.

[12] Doelman, A., Kaper, T. & Promislow, K. (2007) Nonlinear asymptotic stability of the semi-strong pulse dynamics in a regularized Gierer-Meinhardt model. *SIAM J. Math. Anal.* **38**(6), 1760–1789.

[13] Ei, S. (2002) The motion of weakly interacting pulses in reaction–diffusion systems. *J. Dynam. Differential Equations* **14**(1), 85–137.

[14] Ei, S. & Ikeda, H. (2006) *Dynamics of Front Solutions in Reaction–Diffusion Systems in One Dimension*, Preprint.

[15] Frankel, M., Kovacic, G., Roytburd, V. & Timofeyev, I. (2000) Finite-dimensional dynamical system modeling thermal instabilities. *Physica D* **137**(3–4), 295–315.

[16] Ikeda, T. & Nishiura, Y. (1994) Pattern selection for two breathers. *SIAM J. Appl. Math.* **54**(1), 195–230.

[17] Iron, D. & Ward, M. J. (2002) The dynamics of multi-spike solutions to the one-dimensional Gierer-Meinhardt model. *SIAM J. Appl. Math.* **62**(6), 1924–1951.

[18] Iron, D., Ward, M. J. & Wei, J. (2001) The stability of spike solutions to the one-dimensional Gierer-Meinhardt model. *Physica D* **150**(1–2), 25–62.

https://doi.org/10.1017/S0956792508007766 Published online by Cambridge University Press

[19] Kirk, C. M. & Olmstead, W. E. (2005) Blow-up solutions of the two-dimensional heat equation due to a localized moving source. *Anal. Appl. (Singapore)* **3**(1), 1–16.
[20] Kolokolnikov, T., Sun, W., Ward, M. J. & Wei, J. (2006) The stability of a stripe for the Gierer-Meinhardt model and the effect of saturation. *SIAM J. Appl. Dyn. Sys.* **5**(2), 313–363.
[21] Kolokolnikov, T., Erneux, T. & Wei, J. (2006) Mesa-type patterns in the one-dimensional brusselator and their stability. *Physica D* **214**(1), 63–77.
[22] Kolokolnikov, T., Ward, M. & Wei, J. (2006) The stability of spike equilibria in the one-dimensional Gray-Scott model: The low feed-rate regime. *Studies Appl. Math.* **115**(1), 21–71.
[23] Kolokolnikov, T., Ward, M. & Wei, J. (2005) The stability of spike equilibria in the one-dimensional Gray-Scott model: The pulse-splitting regime. *Physica D* **202**(3–4), 258–293.
[24] Kolokolnikov, T., Ward, M. & Wei, J. (2006) Slow translational instabilities of spike patterns in the one-dimensional Gray-Scott model. *Interfaces Free Bound.* **8**(2), 185–222.
[25] Lee, K. J., McCormick, W. D., Pearson, J. E. & Swinney, H. L. (1994) Experimental observation of self-replicating spots in a reaction–diffusion system. *Nature* **369**, 215–218.
[26] Mimura, M., Nagayama, M. & Sakamoto, K. (1995) Pattern dynamics in an exothermic reaction. *Physica D* **84**(1–2), 58–71.
[27] Muratov, C. & Osipov, V. V. (2001) Traveling spike auto-solitons in the Gray-Scott model. *Physica D* **155**(1–2), 112–131.
[28] Muratov, C. & Osipov, V. V. Stability of the static spike autosolitons in the Gray-Scott model. *SIAM J. Appl. Math.* **62**(5), 1463–1487.
[29] Muratov, C. & Osipov, V. V. (2000) Static spike autosolitons in the Gray-Scott model. *J. Phys. A: Math Gen.* **33**, 8893–8916.
[30] Muratov, C. & Osipov, V. V. (2001) Spike sutosolitons and pattern formation scenarios in the two-dimensional Gray-Scott model. *Eur. Phys. J. B.* **22**, 213–221.
[31] Nishiura, Y. & Fujii, H. (1987) Stability of singularly perturbed solutions to systems of reaction–diffusion equations. *SIAM J. Math. Anal.* **18**, 1726–1770.
[32] Nishiura, Y. & Mimura, H. (1989) Layer oscillations in reaction–diffusion systems. *SIAM J. Appl. Math.***49**(2), 481–514.
[33] Nishiura, Y. & Ueyama, D. (1999) A skeleton structure of self-replicating dynamics. *Physica D* **130**(1–2), 73–104.
[34] Nishiura, Y. & Ueyama, D. (2001) Spatio-temporal chaos for the Gray-Scott model. *Physica D* **150**(3–4), 137–162.
[35] Ockendon, J., Howison, S., Lacey, A. & Movchan, A. (2001) *Applied Partial Differential Equations*, Oxford University Press, Oxford.
[36] Park, J. H., Bayliss, A., Matkowsky, B. J. & Nepomnyashchy, A. A. (2006) On the route to extinction in nonadiabatic solid flames. *SIAM J. Appl. Math.* **66**(3), 873–895.
[37] Pearson, J. E. (1993) Complex patterns in a simple system. *Science* **216**, 189–192.
[38] Reynolds, W. N., Ponce-Dawson, S. & Pearson, J. E. (1997) Dynamics of self-replicating spots in reaction–diffusion systems. *Phys. Rev. E* **56**(1), 185–198.
[39] Sun, W., Ward, M. J. & Russell, R. (2005) The slow dynamics of two-spike solutions for the Gray-Scott and Gierer-Meinhardt systems: Competition and oscillatory instabilities. *SIAM J. App. Dyn. Syst.* **4**(4), 904–953.
[40] Tornberg, A. K. & Engquist, B. (2004) Numerical approximations of singular source terms in differential equations. *J. Comput. Phys.* **200**(2), 462-488.
[41] Ueyama, D. (1999) Dynamics of self-replicating patterns in the one-dimensional Gray-Scott model. *Hokkaido Math J.* **28**(1), 175–210.
[42] Vanag, V. K. & Epstein, I. R. (2007) Localized patterns in reaction–diffusion systems. *Chaos* **17**(3), 037110.
[43] Ward, M. J. & Wei, J. (2003) Hopf bifurcations and oscillatory instabilities of spike solutions for the one-dimensional Gierer-Meinhardt model. *J. Nonlinear Sci.* **13**(2), 209–264.
[44] Wei, J. (1999) On single interior spike solutions for the Gierer-Meinhardt system: Uniqueness and stability estimates. *Europ. J. Appl. Math.* **10**(4), 353–378.

https://doi.org/10.1017/S0956792508007766 Published online by Cambridge University Press